UNIVERSITY OF OKLAHOMA

GRADUATE COLLEGE

NOVEL FINITE ELEMENT METHOD TO PREDICT BLAST WAVE TRANSMISSION THROUGH HUMAN EAR

A THESIS

SUBMITTED TO THE GRADUATE FACULTY

in partial fulfillment of the requirements for the

Degree of

MASTER OF SCIENCE

By

KEGAN LECKNESS
Norman, Oklahoma
2016

NOVEL FINITE ELEMENT METHOD TO PREDICT BLAST WAVE TRANSMISSION THROUGH HUMAN EAR

A THESIS APPROVED FOR THE
DEPARTMENT OF BIOENGINEERING

BY

_____
Dr. Rong Gan, Chair

_____
Dr. Vassilios Sikavitsas

_____
Dr. Harold Stalford

Acknowledgements

I would like to thank those in the lab who have assisted my research. First and foremost I would like to thank my advisor, Dr. Rong Z. Gan, director of the Biomedical Engineering Laboratory. Her guidance and discussion was paramount to my growth as a researcher. I would like to thank Dr. Xuelin Wang for his mentorship and providing me his Finite Element Analysis expertise. Finally, I would like to thank Don Nakmali for the great work he did accumulating data during cadaver ear blast experiments. I am quite thankful for being a member of such an outstanding research team.

I would also like to thank the College of Aerospace and Mechanical Engineering for their sponsorship of my teaching assistantships and trips to give oral presentations during the Biomedical Engineering Society Annual Meetings of 2014 and 2015.

My sincerest appreciation to my family for their support and love.

This work was supported by the Department of Defense grant W81XWH-14-1-0028.

Table of Contents

List of Tables

List of Figures

Abstract

As military weapons systems continue to become more powerful, the noise levels they generate become more dangerous to the soldiers deploying them. This has increased the need for advanced methods of evaluating the risks of weapon-generated pressure profiles as well as the need for advanced Hearing Protection Devices to protect against these profiles. The Finite Element Method in conjunction with Computational Fluid Dynamics may be employed in the proposed Human Ear Model to predict human ear response to high-intensity impulse pressures and give insight into earplug function.

This thesis focuses on the development of the first Finite Element model of the human ear for blast impulse analysis. Real-ear geometry was adapted to generate strongly coupled Fluid-Structure Interaction analyses in Fluent/ANSYS Mechanical software. Pressure waveforms measured during human cadaver temporal bone experiments were applied to the model as input; the model was validated by comparing the predicted waveforms monitored at locations within the ear with experimental waveforms measured at identical locations. The model was then applied to explain trends observed during experimentation.

A conceptual model was conceived to investigate the role of orifice geometry in nonlinear earplugs. Then, linear and nonlinear earplugs were introduced to the Human Ear Model for blast impulse analysis.

Chapter 1: Introduction
1.1 Motivation

Tinnitus and noise-induced hearing loss were the most prevalent service-connected disabilities among veterans receiving compensation, accounting for 36% of total cases (20% and 16%, respectively) and over $1 billion [1]. It is estimated that an additional million veterans suffer from service-connected auditory disabilities who do not meet the criteria for compensation [2]; these numbers are only expected to rise, as the percent change in impairment of auditory acuity from 2011-2012 was a 25.6% increase [1].

Noise-induced hearing loss (defined by either temporary or permanent threshold shifts in hearing) has been a concern since the advent of mechanized machinery, artillery, and firearms in war. SPL is usually measured with the logarithmic unit of decibels, where 0 dB SPL is equal to 20 μPa, the auditory threshold in humans; the raised human voice is approximately 76 dB SPL (0.13 Pa). As the need for higher degrees of lethality increases, so must the power, and therefore pressure levels, of weapon systems and platforms. The SPL threshold for pain is commonly known as being 120 dB (20 Pa); the standard 9mm caliber M9 pistol reaches peak SPL of 157 dB (1.42 kPa) measured at the shooter's location [3]. Some weapons, such as the 84mm Multi-role Anti-armor Antipersonnel Weapon System recoilless rifle, generate a massive 190 dB SPL (63 kPa) at the gunner's location. To grant soldiers the maximum degree of lethality while keeping them safe from their own weapon systems and weapon platforms, a comprehensive DRC must be established that is capable of evaluating and accurately predicting human ear response to a wide variety of pressure waveforms. Of specific interest with respect to this thesis is the

ear's response to high-intensity, impulse waveforms, or blasts, which are common amongst firearms, artillery, and explosions, in general.

The U.S. Navy mandates use of single (earplugs or earmuffs) HPDs when exposed to SPLs greater than 85 dB and double HPDs (earplugs and earmuffs) at exposures greater than 105 dB SPL [4]. With double HPDs, wearer is protected against pressure levels under 115 dB; however, aircraft cockpits and carrier decks reach SPLs of up to 135 dB and 150 dB, respectively. On the battlefield, EPs are seldom worn. Although EPs have been developed that allow for attenuation of high-intensity impulse pressures while mildly attenuating important hearing-level communications, promoting situational awareness, these EPs are unpopular due to their uncomfortability and their still-significant loss in communication capabilities. To improve use of HPDs during combat and reduce service-connected ear injuries, the function of current HPDs must be well understood and improved upon.

1.2 Background: Human Ear Anatomy and Function

The human ear is comprised of outer, middle, and inner ear portions. Figure 1 shows a schematic diagram of the human ear. The outer ear is made up of the pinna and external auditory ear canal which terminates at the TM or eardrum. The conical TM, whose apex is termed the umbo, is considered to be part of the middle ear. The manubrium is a soft tissue which attaches the TM to the ossicular chain. The ossicular chain resides within the ME cavity and consists of three ossicles: the malleus, incus, and stapes. The ossicles are separated by joint and are suspended in the ME cavity via suspensory ligaments. The Eustachian tube's primary function is to drain ME fluid and keep ME

pressure at atmospheric levels. The ossicular chain terminates at the oval window of the inner ear, or cochlea. The cochlea houses the organ of Corti, which is comprised of the basilar membrane on which mechanosensory or hair cells reside.

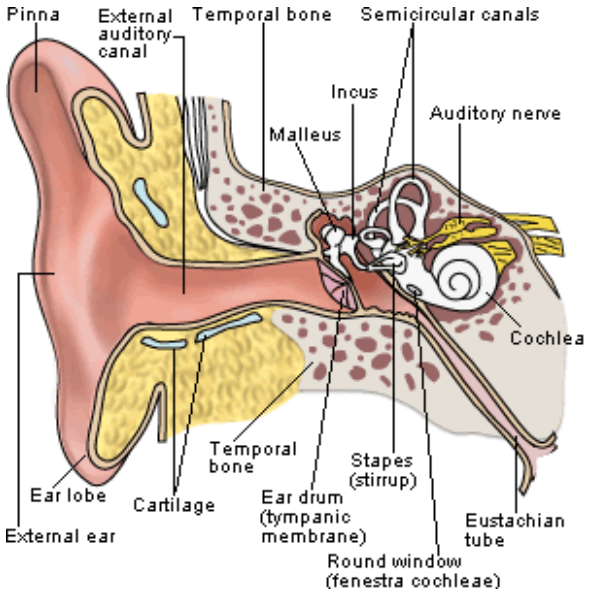

Figure 1: Human Ear Structure (https://s3-ap-southeast-2.amazonaws.com/mydr2016/site_content/files/images/categories/anatom/ear_anatomy.gif)

The primary function of the ear is to transform acoustic vibrations into electrical signals that are transferred by the auditory nerve to the brain. Acoustic vibrations are directed down the external auditory canal by the pinna, which vibrates the TM. This mechanical vibration results in the piston-like motion of the stapes that sets the cochlear fluid into motion; this excites the hair cells within the organ of Corti, which produce electrical signals for the brain to interpret as sound.

1.3 Current Methods for Evaluating Blasts/Earplugs

1.3.1 Auditory Hazard Assessment Algorithm for Humans

In the 1960's, the Army's Human Engineering Laboratory developed MIL-STD-1474 which was adopted as a health hazard criterion for noise exposure by the DoD. By the 1980's, enough research was completed to support the development of a mathematical model of the human ear's response to intense sound, and the AHAAH was created. The AHAAH is an electro-acoustic (circuit) model of the human ear capable of calculating cochlear structural response due to signal transmission from the free sound field outside the ear which has resulted in the development of AHUs [5]. AHUs are the criteria for predicting hearing damage and are determined from the calculated time-history of the displacement, mechanical stress, and number of cycles of the basilar membrane; if the prediction exceeds 500 AHU, permanent hearing loss may occur [6]. The AHAAH model was able to predict the threshold of hazard in better than 95% of cases tested, while MIL-STD-1474D (1997-2015) exhibited only 36% accuracy when examining the same data [7]. In April 2015 the AHAAH model was implemented in establishing the new acoustic noise limits, testing procedures, and DRC described in MIL-STD-1474E.

HPDs are generally divided into two categories: protectors in which the attenuation is constant and does not depend on SPL (usually termed "linear" protectors [8]), and protectors whose attenuation depends on the SPL (usually termed "nonlinear" protectors). Nonlinear HPDs are characterized by their ability to strongly attenuate high-intensity waveforms while only limitedly attenuating hearing-level waveforms. This is achieved via an orifice through the EP whose geometry facilitates dissipative behavior of impulsive and high-level pressure waveforms, while minimally effecting low-level,

harmonic waveforms [8]. The AHAAH model was capable of accurately predicting multiple EP performance in terms of attenuation and general waveform when compared to experiments carried out in an auditory test fixture [9].

The AHAAH model has proven to significantly impact military noise standards through accurate prediction of pressure waveforms and inner ear damage in unoccluded and occluded ears. However, the antiquated approach of circuit modeling significantly limits the details that may be extracted from impulse blast analyses. This electro-acoustic model provides no information of the displacement or stress distributions imparted on the surfaces or throughout the TM or structures of the ME cavity, and only provides such information at discrete points on the basilar membrane. Such detailed information would prove useful in determining criteria for hearing loss due to modes other than cochlear damage – like TM rupture or ossicular chain disarticulation. Although pressure waveforms behind EPs may be predicted, the pressure propagation and distribution throughout the ear canal, ME cavity, and in the fluid domains of the cochlea remain unknown. The transient flow fields may be used to innovate EP orifice design and improve the acceptability of nonlinear EPs amongst soldiers. It is the claim of this thesis that such information missing from the AHAAH model's results may be captured and utilized when conducting analyses using modern FSI capabilities of the FEM.

1.3.2 The Finite Element Method

3-D FSI simulations have proven to be indispensable tools in the evaluation of protective measures against blast injury of human soft tissues. Grujicic *et. al*. at Clemson University, South Carolina utilized FSI analyses and a Finite Element (FE) model of the

human head (helmet, skull, brain assembly) to computationally determine the blast wave mitigation performance of a proposed advanced combat helmet in relation to mild traumatic brain injury [10]. These analyses calculated the complex spatial and temporal evolution of stresses within the brain, with and without helmet, and were used to suggest improvements that enhanced later helmet design [11]. A group from Johns Hopkins University, Baltimore, MD, and the Indian Institute of Technology, Bombay, Mumbai, India utilized a similar approach to analyze eye biomechanics and the protective function of Military Combat Eye Protection [12]. In this study, the function of spectacles and goggles were compared; the transient flow was computed and it was found that, at higher pressure exposures, the goggles trapped air in front of the eye and resulted in sustained elevated pressure loading on the eye higher than even in the unprotected eye case. Both of the referenced studies were funded by the U.S. military, utilized experimental blast data as a tool for model validation, and provided important insight into the function and possible innovation of blast impulse protective equipment.

Sgard *et. al.* at the École de technologie supérieure in Montreal, Quebec, Canada is a leading group in the research of linear (classic foam and custom molded silicon) EP and earmuff function, combining experimentation with FE computational analysis methods. This group has conducted parametric studies [13], [14], [15], [16], studies examining the acoustic impact of ear canal skin [15] and skin with cartilage and bone [13], the occlusion effect [14] and bone conduction occlusion effect [17], acoustic test fixture geometry [16], [14] and over 14 real ear canal geometries [13], [18], and 2-D axi-symmetric models versus 3-D FE models of the ear canal [18]. The limitations of this group's work are that only linear (constant attenuation) EP function has been examined

under low-level pressure (on the order of 120 dB SPL or 20 Pa), harmonic loading conditions in a simplistic ear model.

1.4 The Finite Element Model of the Human Ear

The FE model of the human ear developed in the Biomedical Engineering Laboratory at the University of Oklahoma, Norman, whose geometry was extracted for investigation into the transient realm of blast analyses, has been well-published and has been implemented in the investigation of ear response to numerous conditions. The model, constructed based on a complete set of histological section images of a left ear temporal bone in 2004, was validated by comparing model-predicted displacements at the stapes footplate and TM with published experimental measurements on human temporal bones [18]. It was used in the first FEA of the human ear that featured acoustic-structure coupled behavior between the ear canal air column and the TM and ME ossicles with the air in the ME cavity. As pictured in Figure 2, the HEM featured the fluid domains of the ear canal and ME cavity, the structures of the TM and the TM annulus, the ME ossicles and associated soft joints and suspensory ligaments, and the cochlear load, which modeled the 20 GΩ cochlear impedance applied to the stapes footplate.

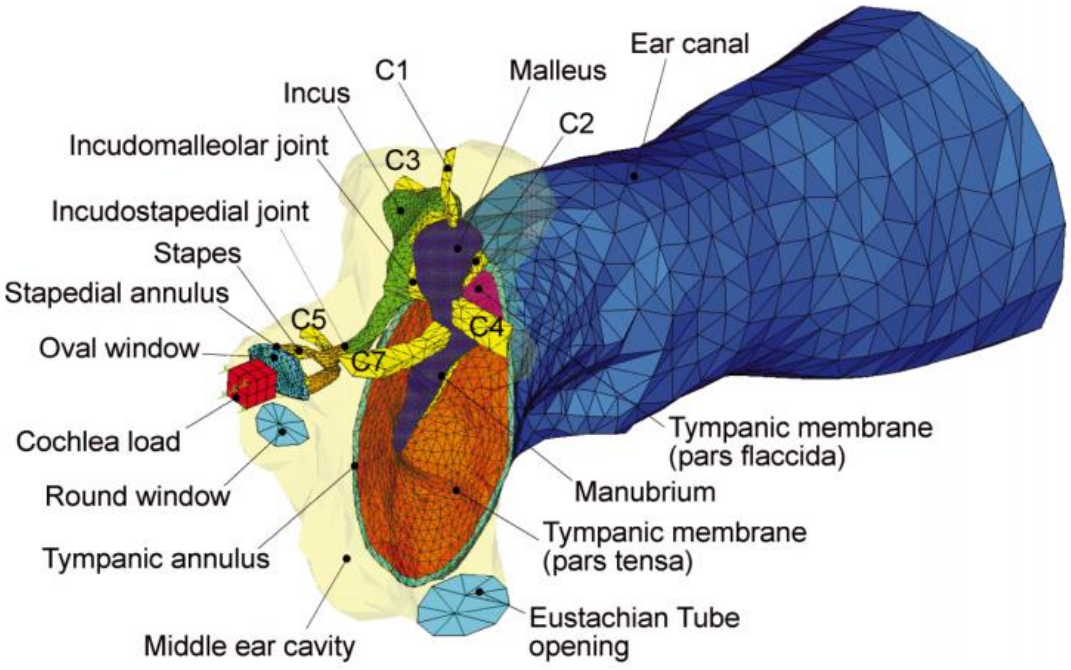

Figure 2: Finite Element Model of Human Ear [19]

In 2007 a hyperelastic material model was applied to the TM and key suspensory ligaments and ME pressure effects on static and dynamic response of the ear was calculated [20]. That same year, a simplified two-chamber straight cochlea with basilar membrane was introduced to the model and sound transmission from the ear canal into cochlea was predicted [21]. This model produced satisfactory agreements between predicted basilar membrane motion and experimental data in literature. This study was the first step toward the development of a comprehensive FE model of the entire human ear for acoustic-mechanical analysis. Another study altered TM geometry to include different numbers and sizes of perforations at particular locations, and the TM displacement and ME pressure were calculated. Cadaver ears were perforated similarly and TM displacement was measured by laser Doppler Vibrometry. Across frequency ranges, the HEM was found to accurately predict TM vibrations and ME pressure levels

when compared to experimental measures [22]. In a later iteration of the HEM, viscoelastic material properties and a three-chamber spiral cochlea were introduced. This study showed the model's capability of modeling energy absorbance in normal ears and ear with otitis media, otosclerosis, and ossicular chain disarticulation [23]. The model has also been implicated in evaluating totally implantable hearing systems [24].

Over the past ten years, the HEM has proven to be a valuable tool when used in conjunction with experimental data, capable of predicting ear function from canal to cochlea, various modes of ear damage and disease, and even the behavior of implantable biomechanical systems. The analyses discussed above were conducted ANSYS APDL and investigated ear function in low-pressure conditions in the frequency domain. In this thesis, the geometry of the previous HEM model was extracted and modified to create new models for the analysis of mid- and high-level impulse pressure waveforms in short-scale transient domain analyses.

1.5 Objectives

Because the impact blast-related tinnitus and hearing loss have on the quality of life of affected soldiers and society is so great, our understanding of the causes and risks of ear damage and the capability of HPDs must be improved. Towards this, further research in two primary directions is needed: 1) Damage Risk Criteria (DRC) must be derived from analysis methods with the ability to predict stresses and fatigue of all important ear components under a multitude of impulse and steady noise conditions; and 2) EP design must be advanced such that they provide sufficiently high degrees of attenuation for impulsive and otherwise high-pressure waveforms while minimally

reducing soldiers' combat effectiveness and communication capabilities. To achieve this, an advanced analysis scheme is needed. Toward devising such analysis scheme capable of providing detailed structural response of ear components as well as the transient flow profile of air through the ear, strongly coupled FSI analyses using the updated HEM in the Fluent/ANSY Mechanical environment were conducted. Insights from these analyses may be used to predict TM damage under blast loading and optimize design of nonlinear earplugs.

1.5.1 Outline

Implementation of Human Ear Model predictions of blast impulse

- The HEM is transferred into ANSYS Workbench where the fluid and structural components are divided into analysis software Fluent and ANSYS Mechanical, respectively.
- Appropriate boundary conditions, material properties, and fluid-structure interfaces are applied.
- The analyses are initiated through application of experimental blast waveforms measured outside of cadaveric ears.
- The predicted waveforms at key locations are compared against experimental waveforms at same locations.
- Validated HEM is then applied to posit explanations for trends seen amongst experimental blast groups (Vertical, Horizontal, and Front).

Initial parametric study of linear and nonlinear Hearing Protection Devices

- A conceptual model is created for parametric study and is validated against HEM.

- Foam EP material properties are examined.
- Multiple geometries are created to test effects of EP insertion depth and orifice configuration subjected to impulse loading.
- Waveform differences resulting from varying EP geometries are discussed.

Human Ear Model is implemented in earplug analysis

- The HEM is modified to create unoccluded and occluded EP (foam and Combat Arms triple-dome-only) models.
- Mid- and high-level blast waves from unoccluded and occluded cadaver ear experiments are used to initialize model computation.
- Model predictions are compared against experimental measures and are discussed.

Chapter 2: Finite Element Analyses of Human Ear Response to Blast Impulse

The FE analyses of the HEM previously reported in literature utilized the computational software ANSYS APDL (or ANSYS Classic) to predict the middle ear response under numerous conditions in the frequency domain. ANSYS APDL solved, both, the structural response of the TM, ME structures, and cochlear load, as well as the fluid response of the air in the ear canal and ME cavity. The acoustic fluid element type FLUID30 was used to calculate the acoustic pressure propagation down the ear canal and throughout the ME cavity via the 3-D wave equation. This element type had several limitations when evaluating its feasibility of being implemented in blast wave analyses: analyses with this element type were limited to small acoustic pressures, its linear shape function did not well represent complicated pressure distributions in the fluid chambers, and the governing wave equation did not sufficiently model a blast's impulse waveform. Therefore, an enhanced solver method was needed for blast analyses. Geometry was adapted from the previously reported HEM for use in the current 3-D HEM.

This chapter will discuss the newly created HEM model for the analysis of blast impulse transmission. The newly implemented analysis software will be discussed and solver methodology will be detailed. Material assumptions and boundary conditions will be described. Model validation rational will be presented, and then the model will be applied to examine trends seen in cadaver ear blast experiments.

2.1 ANSYS Workbench: Coupled Analyses

When founded, ANSYS was solely a structural solver; after numerous industry buyouts, ANSYS Inc. is now the global leader in engineering simulation, capable of

structural, fluids, electronics, heat transfer, electromagnetic, explicit dynamics, and multiphysics analyses. This section will provide an overview of the solution methodology of Fluent/ANSYS Mechanical coupled analysis. ANSYS Workbench provides the project-level control necessary to easily create a custom and comprehensive analysis system by providing drag-and-drop system modules that allow for the geometry creation, mesh generation, analysis setup and monitoring, and post-processing for all of the programs in the Workbench suite. Figure 3 shows the analysis system created for the blast simulations in the HEM.

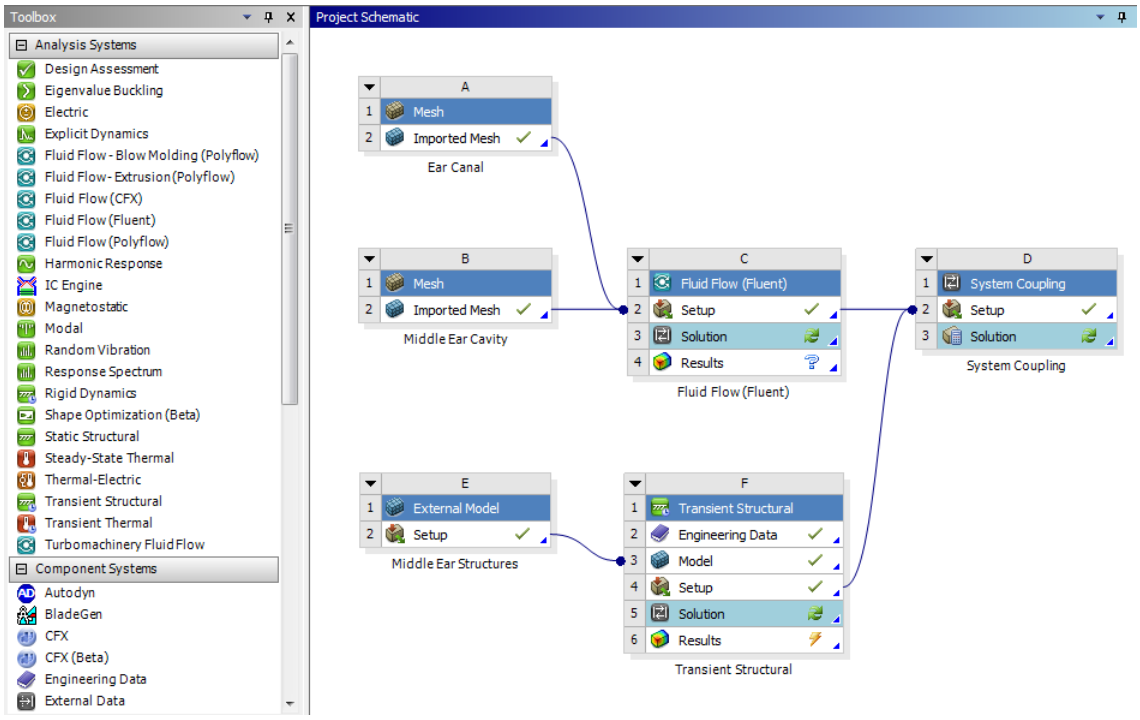

Figure 3: The ANSYS Workbench Project Schematic showing the flow of data from the mesh readers to the analysis systems to the coupling service. [25]

The analysis software implemented to deliver the desired simulation system were Fluent and ANSYS Mechanical, which solved the fluid and structural domains,

respectively. .MSH files containing the ear canal and ME cavity meshes were read by individual Mesh component systems before being transferred to Fluent; the External Model component system was used to read in the .CBD structural mesh file, which included the TM, TM annulus, ossicular chain and associated suspensory ligaments, and cochlear load, and feed the mesh to ANSYS Mechanical. The individual solver principles and analysis settings will be discussed in following sections.

In order to accurately model the physics of high-intensity impulse pressure propagation down the ear canal and its interaction with the ME structure, Fluent and ANSYS Mechanical must be able to communicate with one another bi-directionally. This is achieved through application of strongly coupled FSIs that are facilitated by the Workbench component system, System Coupling. Strongly coupled FSIs are prescribed by application of fluid-structure interfaces, which must be specified on coincident mesh faces in both Fluent and ANSYS Mechanical (e.g. on the canal's interface with the TM and on the TM's interface with the canal). The execution sequence diagram for the System Coupling service is shown in Figure 4.

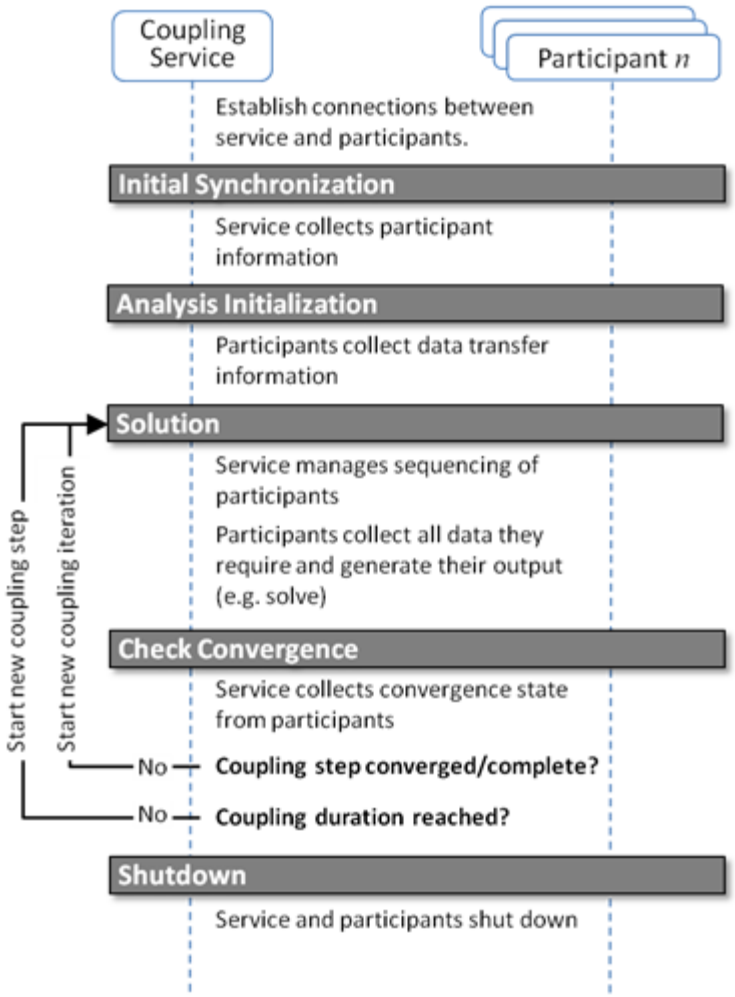

Figure 4: The execution sequence diagram for the System Coupling service and the involved solver participants. [26]

Shown in dark gray are the synchronization points which act as a gateway beyond which an analysis will not progress until all necessary processes or sub-processes have successfully completed. After the coupling service and solver participants are connected, Initial Synchronization must be achieved; at this point, the meshes and analysis settings of the involved participants are collected. The analysis is initialized when the data containing the initial conditions of all involved participants are transferred across the

fluid-structure interfaces (e.g. the fluid pressure distributions of the ear canal and ME cavity on their shared surfaces with the TM are transferred to the TM structure at t = 0 s.)

The solution synchronization point is passed once the appropriate data transfers between the participant programs and the subsequent solving of each participant is complete at each time step and coupling iteration. After each iteration is solved, convergence is checked for each participant; if the time step has not yet converged, a new coupling iteration initiates and the solution synchronization begins again. After convergence of a single time step is reached, the loop continues until all time steps making up the analysis duration are complete or divergence is detected and the analysis fails. Upon analysis completion, the coupling service and participants are shut down.

For a given analysis duration (say, 2 ms), the user defines a time-step size (say, 1 μs); in this case, the analysis is comprised of 2,000 time steps. For the first time step after the analysis has been initialized, the solution method for Fluent/ANSYS Mechanical analyses follows. During the first iteration of the first time step, Fluent calculates the pressure distribution throughout the fluid domains based on its input and passes the calculated forces onto the fluid-structure interfaces, via System Coupling. ANSYS Mechanical then solves the response of the structure under any applied loads and those passed to the structure from Fluent. The convergence check is failed, and ANSYS Mechanical passes its displacement information to Fluent. A new iteration begins in which Fluent recalculates the pressure distribution with respect to the new domain shape stemming from the structural deformation. The updated pressure forces are passed back to ANSYS Mechanical, which solves the updated structural deformation. This iterative

process continues until convergence of both solvers are reached; then the analysis moves on to the next time step until analysis completion.

After analysis completion, Workbench offers multiple options for results post-processing. Within ANSYS Mechanical, component-specific displacement, stress, and strain distributions may be viewed. The component system CFD-Post allows for the visualization of the pressure and velocity distributions within the fluid domains. This list results is not comprehensive, but are the output parameters that will be discussed later within this document.

2.2 Generating Model for Blast Simulations

The previous section discussed the application of ANSYS Workbench and explained the strongly coupled FSI analysis method. The current section will give insight into solver methodology and will detail the analysis settings used in both Fluent and ANSYS Mechanical for the purpose of simulating high-intensity pressure propagation through the Human Ear Model.

2.2.1 Fluent Methodology

Fluent is one of the world's largest commercial CFD providers that offers a wide array of advanced physical models [27]. CFD is a subset of fluid dynamics that uses numerical methods to approximate solutions for fluid flow problems. In this approach the fluid domain is discretized, which results in a system of equations at nodal locations that when solved give a discrete representation of the solution. Fluent uses the FVM, in which the governing conservative PDEs are implicitly solved over discrete control volumes

(cells); this conservative form means that the flux exiting one cell is equal to the flux entering the next. The FVM is common across CFD codes, as it requires less memory usage, results in faster solve times, and is more conducive to a conservative solution approach compared to the FEM [28].

2.2.1.1 Equations Used to Predict Pressure Propagation in Human Ear Model

The constitutive equations Fluent employs to solve fluid flow problems are generally referred to as the Navier-Stokes equations. The Navier-Stokes equations consist of the continuity and momentum equations (that are standard equations solved by Fluent), the energy equation (necessary for flows involving heat transfer or compressibility), and the ideal gas law for compressible flows; turbulence effects are not considered in the current HEM analyses.

Equation **(1)** is the 3-D continuity equation, also called the mass conservation equation, and is valid for incompressible as well as compressible flows.

$$\frac{\delta \rho}{\delta t} + \nabla \cdot (\rho \vec{v}) = S_m \qquad \textbf{(1)}$$

ρ is the density and $\vec{v}$ is the velocity vector . S_m is a source term representing the mass added from phase change or any user-defined sources [29]; in the case of the HEM analyses, there is no source term and S_m is zero.

The momentum equation of a non-accelerating reference frame is described by equation **(2)**.

$$\frac{\delta}{\delta t}(\rho\vec{v}) + \nabla \cdot (\rho\vec{v}\vec{v}) = -\nabla p + \nabla \cdot (\bar{\bar{\tau}}) + \rho\vec{g} + \vec{F} \quad \textbf{(2)}$$

In this equation, p is the static pressure, $\rho\vec{g}$ is the gravitational body force, and $\vec{F}$ is the external body forces [29]. Gravitational effects are ignored, and thus $\rho\vec{g}$ is zero. The pressure waveform applied to the entrance of the ear canal (discussed later) is accounted for by the external body forces. $\bar{\bar{\tau}}$ is the stress tensor and is given by equation **(3)**

$$\bar{\bar{\tau}} = \mu[(\nabla\vec{v} + \nabla\vec{v}^T) - \frac{2}{3}\nabla \cdot \vec{v}\, I \quad \textbf{(3)}$$

where μ is the molecular viscosity of air, I is the unit tensor, and $\nabla\vec{v}^T$ is the effect of volume dilation [29].

The energy equation is given by equation **(4)**.

$$\frac{\delta}{\delta t}(\rho E) + \nabla \cdot \left(\vec{v}(\rho E + \rho)\right) = \nabla \cdot \left(k_{eff}\nabla T\right) + S_h \quad \textbf{(4)}$$

Here, E is energy, k_{eff} is the effective thermal conductivity, and S_h is the source term that contains contribution from radiation and other volumetric heat sources [29] [30]; S_h is zero.

An equation of state is necessary to close the above equations. This is achieved through the application of the ideal gas law for compressible flows; expressed by equation **(5)**.

$$\rho = \frac{p_{OP} + p}{\frac{R}{M_w}T} \quad \textbf{(5)}$$

p_{OP} is the operating pressure of the analysis, R is the universal gas constant or 8.314472 (J/mol-K), and T is the absolute pressure computed from the energy equation [28].

2.2.1.2 Fluid Analysis Setup

The objective of the analysis setup process is to apply the appropriate loads and boundary conditions, under the proper assumptions, that will result in the most accurate representation of the physics of the physical system of interest. Fluent version 16.1 was chosen for this transient, compressible, laminar fluid flow analysis. Compressible flows are often characterized by the value of their Mach number, which is the ratio of the velocity in a system over the speed of sound in that gas; when the Mach number is less than 1.0, the flow is termed subsonic and may be considered incompressible. At sufficiently high Mach numbers (approximately > 0.1) compressibility effects are no longer negligible, meaning the density of the gas varies with pressure, and cannot be ignored in analyses. Compressibility effects must also be taken into consideration in circumstances in which there are abrupt and dramatic changes in pressure level. As a subsonic blast wave of around 40 kPa enters the ear canal its velocity corresponds to a Mach number of approximately 0.3, and thus compressibility were included in the analyses. Although at the entrance of the ear canal the entrance velocity is significant (i.e. total pressure is comprised of both static and dynamic pressures), total pressure measured at the end of the canal is comprised almost entirely of static pressure. Thus, as the pressure propagates down the 30x8 mm cylindrical canal, the pressure front rapidly loses velocity and may be sufficiently represented by laminar flow.

An important parameter in CFD simulations is what is known as the Courant number. The Courant is given by equation **(6)** and represents how the flow is moving through the mesh [31].

$$C = \frac{u\Delta t}{\Delta x} \quad \textbf{(6)}$$

It is determined by the flow velocity, time step size, and element size in the direction of flow. If the Courant number is <= 1, this means that the fluid flow moves from one cell to the next within one time step (at most); if the Courant number is > 1, the fluid flow moves through more than one cell with each time step, possibly resulting in a divergent solution. The cell size of the ear canal get smaller approaching the TM, as does the velocity. A time step size of 1 μs results in an average Courant number of approximately 0.1, suggesting the mesh cell size will provide a satisfactory level of flow resolution.

Standard compressible air properties were employed and the operating pressure was set to ambient air pressure at sea level, or 101,325 Pa. Gravity effects were neglected. As the TM deformed greatly under high pressure, so must fluid-structure interfaces the canal and ME cavity fluid domains. To keep the fluid meshes' cell quality sufficient for convergence under conditions of large deformation, a dynamic smoothing and remeshing scheme was employed. The smoothing scheme allowed interior fluid nodes to absorb the motion of nodes directly adjacent to the moving FSI boundaries, which prevented negative cell volumes. When the mesh deformation was significant enough, the remeshing scheme was activated, which allowed for local or region remeshing mid-analysis. The remeshing scheme greatly enhanced the solvability of these analyses, and was ultimately why Fluent was chosen over other CFD packages for this application.

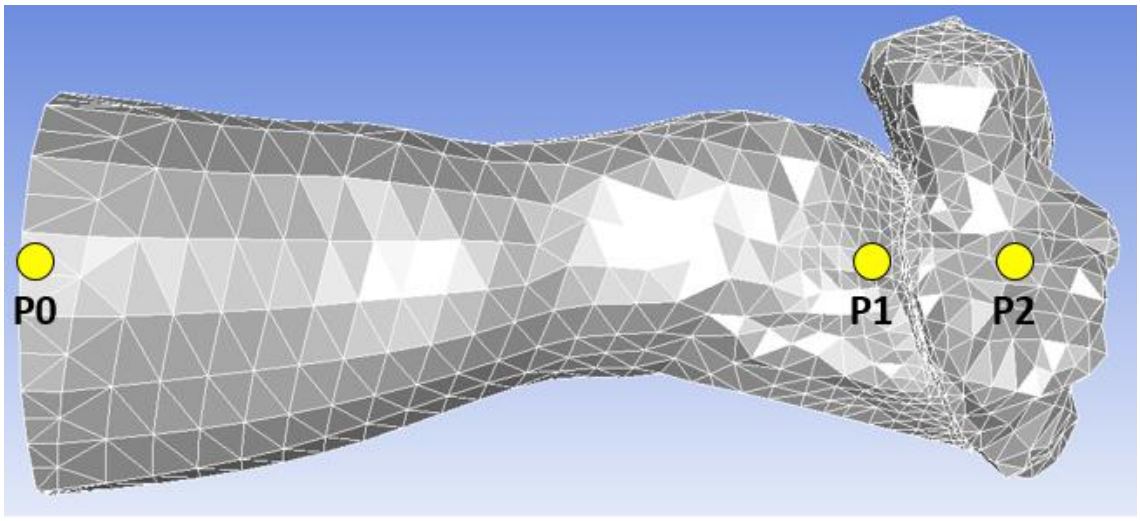

Figure 5: Ear canal and ME cavity fluid domains in Fluent. Pressure monitor locations P0, P1, and P2 are shown at the entrance of the canal, just before the TM, and within the ME cavity, respectively.

Correct application of boundary conditions is key for proper analysis. The entrance of the ear canal was defined as a pressure-inlet. Here, experimentally measured P0 waveforms were applied as the input which drove the analyses. The walls of the ear canal and ME cavity were defined as rigid, no slip walls. Two separate fluid-structure interfaces were applied, one to either side of the TM. These were necessary to pass the fluid forces acting on these surfaces to the structure and to receive the structural displacements under these loads. The FSI between the ossicular chain and air within the ME cavity was ignored due to the high additional computational requirements that resulted in little change in pressure magnitude within the ME cavity.

The analysis duration was set to 2 ms. The desired output of the analyses were the pressure waveforms predicted at locations P1 and P2, on the lateral and medial side of the TM, respectively, as shown in Figure 5. Therefore, static pressure monitors were initialized at these locations, although the full pressure and velocity fields were calculated at each time step.

2.2.2 Structural Analysis in ANSYS Mechanical

ANSYS Mechanical employs the FEM to approximate solutions to boundary value problems for PDEs. In the scope of this paper, the FEM involves discretizing the complex geometry of the ME components into simpler parts, called elements. The structural mechanics equations are solved at each element based on the global boundary conditions, material properties, and element shapes; the element equations are then systematically combined into a global system of equations for final calculation at each time step iteration. ANSYS Mechanical provides an enhanced, easy-to-use graphical user interface as compared to ANSYS APDL, but the solver equations are identical. An in-depth discussion of the solver tactics of ANSYS Mechanical will not be included in this thesis, as they are largely the same as those reported in the literature of the previous human ear models. This section will focus on the analysis setup for the HEM blast analyses.

2.2.2.1 ANSYS Mechanical Analysis Setup

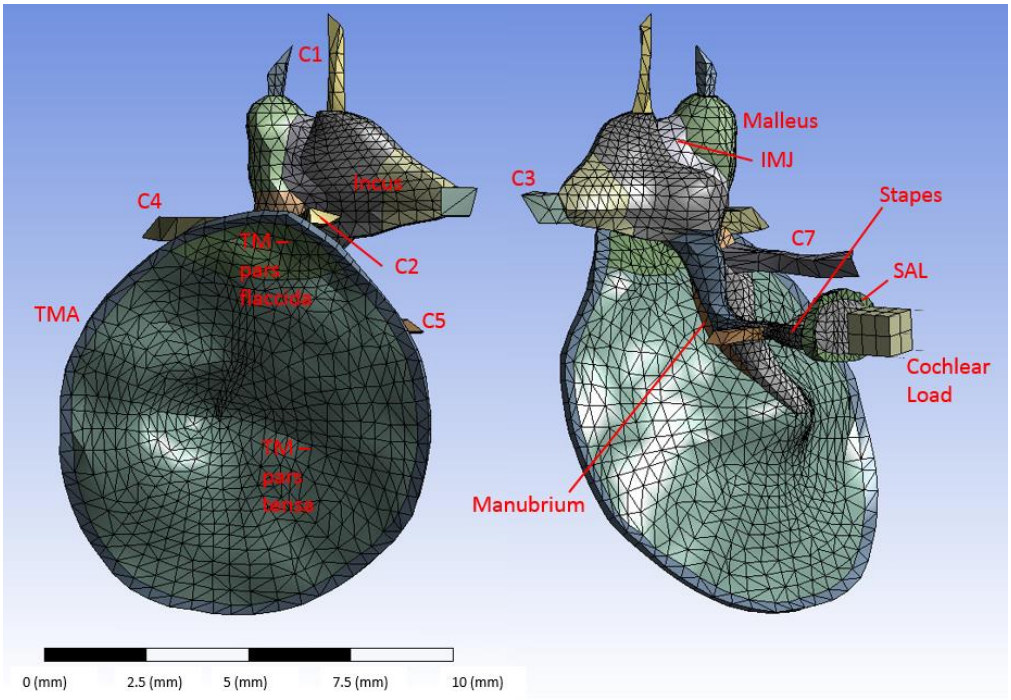

Figure 6: Mesh of Middle Ear structures with labeled components.

Three element types were used in the HEM analyses – those were the 8-node hexahedral elements of the cochlear mass, the 6-node prism elements of the TM (pars tensa and pars flaccida) and TMA, and the 4-node tetrahedral elements of the manubrium, ME ossicles, IMJ, ISJ, and SAL. Also comprised of tetrahedral elements were the superior mallear, lateral mallear, posterior incudal, anterior mallear, posterior stapedial, and tensor tympani ligaments and tendons, or C1, C2, C3, C4, C5, and C7, respectively. (Components shown in Figure 6.) Three degrees of freedom exist at each node: translation in the x, y, and z directions. The elements exhibit viscoelasticity, large deflection, and large strain capabilities. Ten 1-D dashpots were used for the modeling of the damping of the cochlear load; five connecting the cochlear mass to the stapes footplate and five connecting the cochlear mass and ground.

The analysis duration was set to 2 ms with a time step size of 1 μs, as in Fluent. The duration was deemed long enough to observe the development of the pressure waveforms in the ear canal and ME cavity, as well as the initial response and subsequent vibration of the TM and ME structures. The time step size was found to be small enough to resolve the structural displacements under high-intensity pressure loading.

The material properties used in the HEM analyses were adapted from literature. In most FE models of the middle ear, the Young's modulus of the ME tissues were assumed constant and frequency independent [20] [32]. The Poisson's ratio was assumed 0.3 for the entire system. The density of the ME ligaments was assumed 1000 kg/m^3 as in previous studies [20] [21]. Ossicular densities were averaged across their constituent parts (e.g. malleus head, neck, and handle). Governed by Hooke's Law, the following components were considered linear elastic materials: the manubrium, ossicles and suspensory ligaments, and the cochlear mass. The elastic materials are given in Table 1.

Table 1: Elastic material properties used in HEM [19]

Structure	Density (kg/m^3)	Young's Modulus (N/m^2)
Manubrium	1000	4.9×10^9
Malleus	3600	1.41×10^{10}
Incus	3230	1.41×10^{10}
Stapes	2200	1.41×10^{10}
Cochlear Mass	3600	8×10^{10}

Ligaments	Young's Modulus (N/m^2)
Superior mallear ligament (C1)	4.9×10^6
Lateral mallear ligament (C2)	6.7×10^6
Posterior incudal ligament (C3)	6.5×10^6
Anterior mallear ligament (C4)	2.1×10^7
Posterior stapedial tendon (C5)	5.2×10^7
Tensor tympani tendon (C7)	7.0×10^7

Linear viscoelastic material parameters of the TM (pars tensa and pars flaccida), TMA, IMJ, ISJ, and SAL were adapted from those reported in [23]. Here, the standard linear viscoelastic model was used with the relaxation modulus of the tissues being expressed as equation **(7)**.

$$E(t) = E_0 + E_1 \exp(-\frac{t}{\tau_1}) \quad \textbf{(7)}$$

In ANSYS, linear viscoelasticity is modeled by combining linear elasticity with Prony Shear Relaxation. One-parameter Prony Shear Relaxation is given by equation **(8)**.

$$G(t) = G_0[a_\infty^G + a_1^G \exp\left(-\frac{t}{\tau_1}\right)] \quad \textbf{(8)}$$

Here, G_0 is the relaxation modulus at t = 0 and a_1^G is the relative modulus, i.e. it is the portion of G_0 that trends to zero as time approaches infinity. τ_1 is the relaxation time and represents how quickly this relaxation occurs. Prony Shear Relaxation is defined by the relaxation time and the relative modulus.

Since the elastic modulus and shear modulus are linearly related by equation **(9)**, the experimentally obtained viscoelastic properties reported in [23] may be directly applied to yield the appropriate relaxation modulus and relative modulus. Table 2 gives the viscoelastic material properties used in this thesis. The strength of the TMA was artificially increased by a factor of approximately 20 to maintain its integrity during high-intensity impulse pressure loading; this is not thought to significantly affect the predicted pressure magnitudes.

$$E = 2G(1 + \nu) \quad \textbf{(9)}$$

Table 2: Material properties of the viscoelastic soft tissues

Soft tissues	E_0 (MPa)	E_1 (MPa)	τ_1 (μs)	Density (kg/m^3)
TM-PF	7	16	25	1200
TM-PT	25	70	25	1200
TMA	14	46	25	1200
IMJ	60	180	20	3200
ISJ	0.4	20	20	1200
SAL	2.0	10.8	24	1200

The structure of the middle ear responds passively to the fluid pressure acting on it. Fixed boundary conditions around the TM annulus and where ligaments meet the bony structure of the ME cavity suspend the ME structures. A fluid-structure interface on the lateral (canal side) side of the TM receives pressure input, driving the initial response of the ME structures. The FSI between the medial side of the TM and the ME cavity transmits pressure into the middle ear, generating the P2 reading.

2.3 Results and Validation

FEA is an integral instrument in the development of solutions to complex engineering problems. A validated FE model can be used to probe what cannot be examined experimentally and may be used to test the feasibility of various product designs that would be too expensive to physically produce and test. The versatility and accuracy of FE analyses makes them an important tool in research in academia and industry.

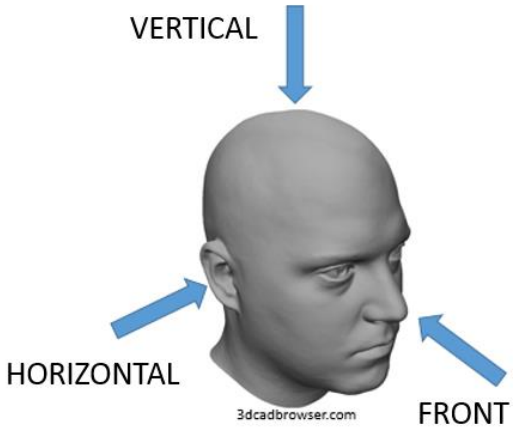

Figure 7: Blast orientation visualization with 3-D model head

The HEM was considered validated for blast wave propagation analyses when it was able to accurately predict experimentally measured waveforms at locations near the TM when driven by experimentally measured waveforms surveyed outside of the ear canal. Cadaver temporal bone experiments were conducted in the Biomedical Engineering Laboratory's Free Field Blast Chamber at the University of Oklahoma in Norman to determine TM rupture thresholds when high-intensity blast waves are oriented in the Vertical (N=14), Horizontal (N=14), and Front (N=14) directions with respect to the mounting headblock; visualization provided in Figure 7. The blasts resulted in pressure propagation that was captured by pressure sensors at P0, outside of the ear canal, P1, just in front of the TM, and P2, inside of the ME cavity, as shown in Figure 5. A total pressure sensor is set perpendicular to the oncoming blast wave and measures P0. The P1 and P2 sensors measure static pressure at their locations. An example of the experimental results is shown in Figure 8.

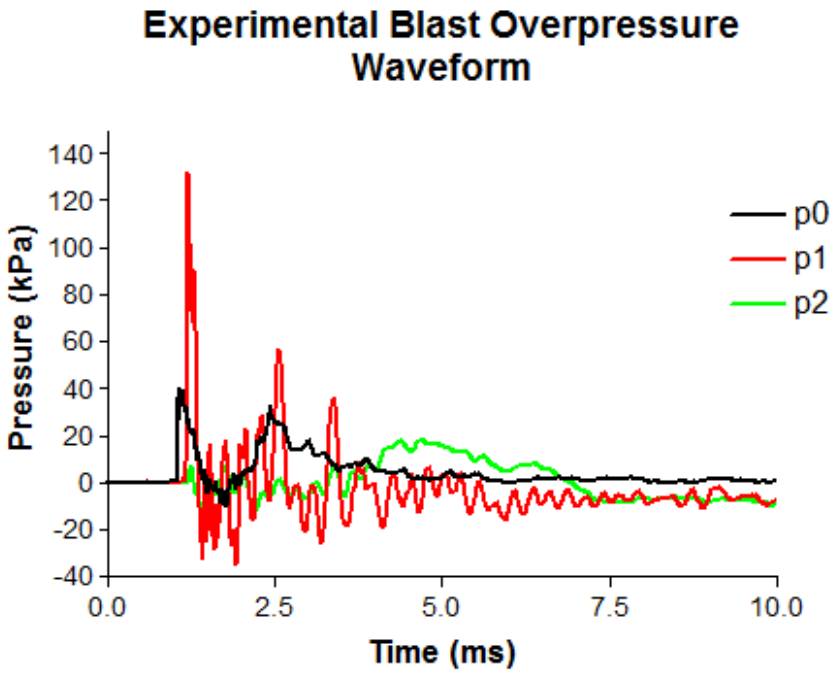

Figure 8: An example waveform resulting from cadaver ear temporal bone experiments. The P0, P1, and P2 pressure waveforms were taken near the entrance of the ear canal, just before the TM, and inside of the ME cavity, respectively.

The total pressure measured at P0 is amplified near the TM at P1, where the static pressure waveform is registered. TM rupture and damage was caused by the P1 waveform; therefore the effect, P1, to the cause, P0, is the main focus of this study; discussion of P2 is included for completeness. In addition to the peak pressure levels of P0 and P1, the amplification ratio, P1/P0, is important for discerning the differences blast orientation has on TM rupture threshold. The rupture threshold level was determined by incrementing the blast wave intensity until rupture was observed, and is defined as the maximum pressure the TM can undergo prior to failure.

Three experimental P0 waveforms from the Vertical, Horizontal, and Front directions were applied to the entrance of the ear canal in Fluent for full FSI analyses,

and the resulting P1 and P2 predictions were compared to the experimental waveforms. The comparison is shown in Figure 9.

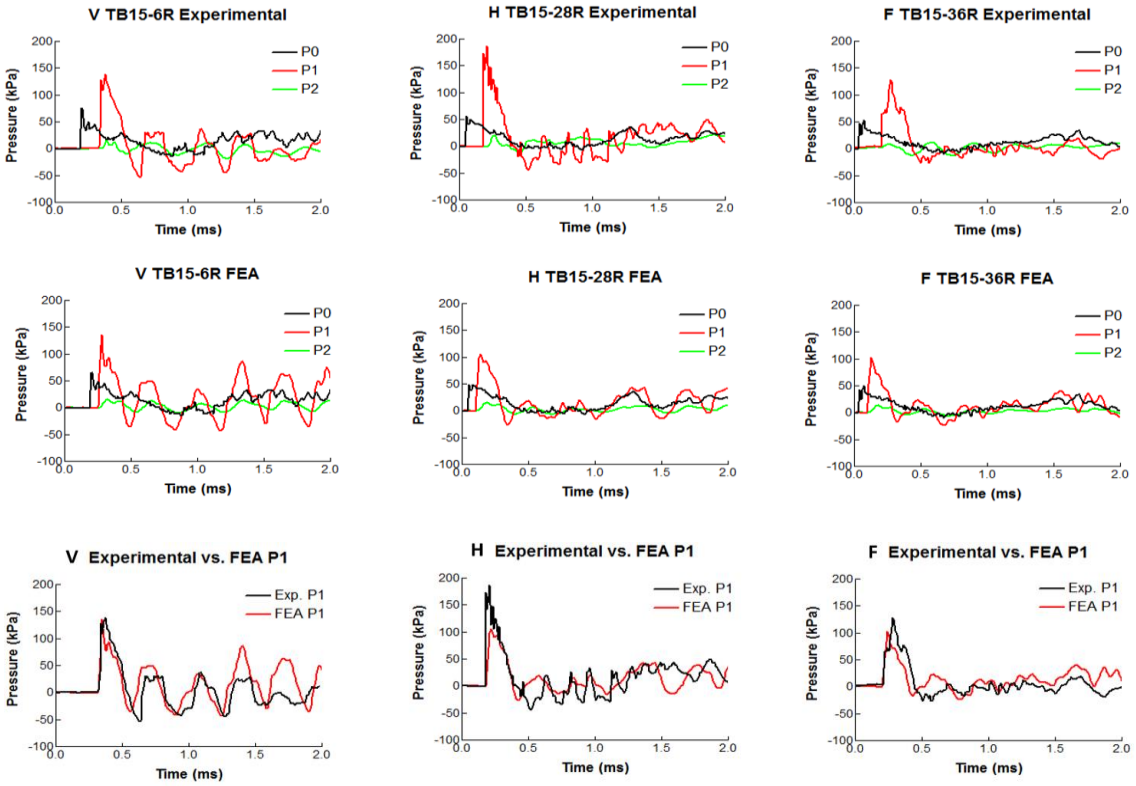

Figure 9: Comparison of the experimental and FEA predicted waveforms for the Vertical, Horizontal, and Front directions. (Top) Experimental waveforms. (Middle) FEA predicted P1 and P2 waveforms with experimental P0 used as input. (Bottom) Comparison P1 vs. P1

The factors that contribute to P1 waveform are entrance pressure magnitude, entrance velocity, ear canal and pinna (outer ear) geometry, and the P0 waveform, itself. Therefore, a qualitative assessment was conducted to determine the predictability of the newly created HEM for blast transmission. As shown in the figure above, the model was successful in predicting P1 and P2 waveform and peak magnitudes. In all cases, the predicted P1 level was lower than the experimental values, however this difference was

only pronounced for the Horizontal case. Comparing FEA-derived with experimental P1 waveforms shows the model has the ability to accurately predict the shape of P1 and P2 given P0 input.

A primary advantage the FE method has over the circuit analysis method for blast analysis in the human ear is the ability to derive structural displacement and stress distributions (an example of which is shown in Figure 10).

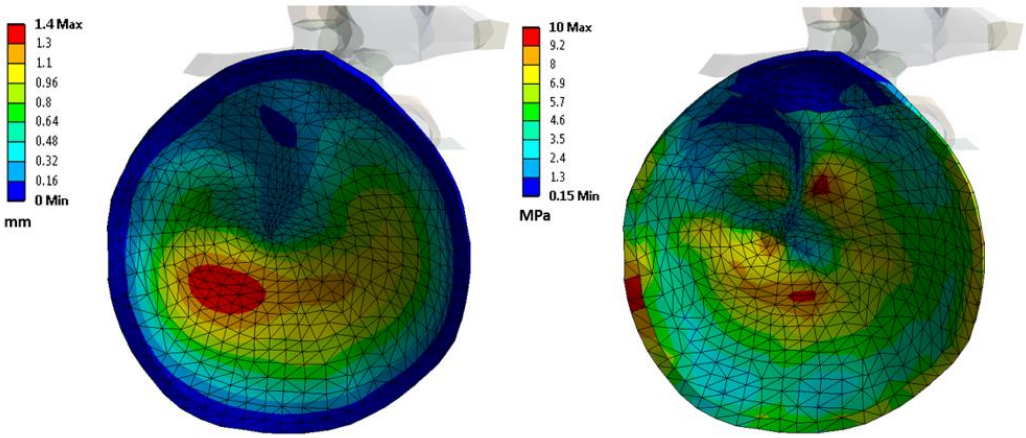

Figure 10: Example of structural distribution results available in the Finite Element Method. (Left) Displacement distribution at time of max; and (Right) stress distribution at time of max.

The left and right images in the above figure show the distribution of maximum displacement taken at time of maximum displacement and the distribution of maximum stress taken at time of maximum stress, respectively. Analyses with the FE method provide the capability of predicting the mode of TM rupture for specific geometries, and predict ear response in much greater detail as compared to circuit analysis. It should be noted, however, that the current TM is modeled as an isotropic solid, when in reality it is

a complex three-layered structure; to best predict TM rupture mechanics, TM geometry must be modified to include the epithelial, mucosal, and fibrous layers.

2.4 Application of the Human Ear Model

Once the HEM was demonstrated as being capable of accurately predicting experimentally measured waveforms it was employed to explain some trends observed in the experimental data. The results investigated are given in Table 3.

Table 3: Experimentally determined blast TM rupture thresholds.

Direction	P0 Rupt. Thresh.	P1 Rupt. Thresh.	P1/P0
V (N=14)	63 ± 12 kPa	131 ± 23 kPa	2.2 ± 0.5
H (N=14)	44 ± 14 kPa	131 ± 41 kPa	3.4 ± 0.7
F (N=14)	67 ± 15 kPa	112 ± 22 kPa	1.7 ± 0.4

In the above table, the P0 Rupture Threshold is defined as the maximum P0 pressure level reached prior to TM rupture. The P1 Rupture Threshold is considered the maximum pressure value the TM can withstand without rupture. Two trends were observed: 1) the P1 Rupture Threshold for the Front direction was approximately 20 kPa lower than both the Vertical and Horizontal direction; and 2) the P0 Rupture Threshold for the Horizontal direction was lower than the Vertical and Front directions, which were approximately equal. The HEM analysis strategies described earlier in this chapter were used to provide explanation for these trends. This section will highlight the initial contributions of the HEM for blast impulse analysis.

2.4.1 Explaining Front Direction P1 Rupture Threshold Level

TM geometry and material properties of the 42 temporal bones tested were assumed to be equal; therefore, it should be expected that all tested TMs would have similar P1 rupture thresholds. As shown in Table 3, blast overpressure from the Front direction with respect to the experimental headblock resulted in TM failure at lower pressures than the Vertical and Horizontal blast orientations (whose P1 rupture thresholds are approximately equal). This suggested that the Front P1 waveform interacted with the TM dissimilarly than P1 waveforms from the other directions. In a study in chinchillas, TM mechanical damage was examined in relation to impulse pressure waveform, and it was found that the resulting stress gradient with respect to pressure characterized TM damage induced by blast [33]. Thus, it was hypothesized that the Front direction P1 waveforms imparted a larger stress gradient with respect to P1 pressure than the Vertical and Horizontal P1 waveforms.

To investigate the stress gradients (i.e. rate of change of maximum stress with respect to maximum P1 pressure, $d\sigma_{max}/dP1$) resulting from the P1 waveforms from the three blast orientations, ANSYS Mechanical was employed in structure-only analyses. P1 data from four samples from each blast orientation were applied directly to the surface of the TM so as to avoid the inherent calculation error as Fluent simulated the pressure propagation down the ear canal; the objective was to examine experimental P1 effect. Having used experimental P1 waveforms as structural load input, the stress distributions across the TM were predicted.

Identical material properties and boundary conditions (with the exception of fluid-structure interfaces) were applied to the structure during this set of analyses, as discussed

previously. The analysis methodology for determining the stress gradients on the TM resulting from the three blast orientations follows:

1. Four sets of incremental blast data measured at P1 were obtained from the Vertical, Horizontal, and Front blast orientations. An example set of such data for the Vertical direction is given by Figure 11.

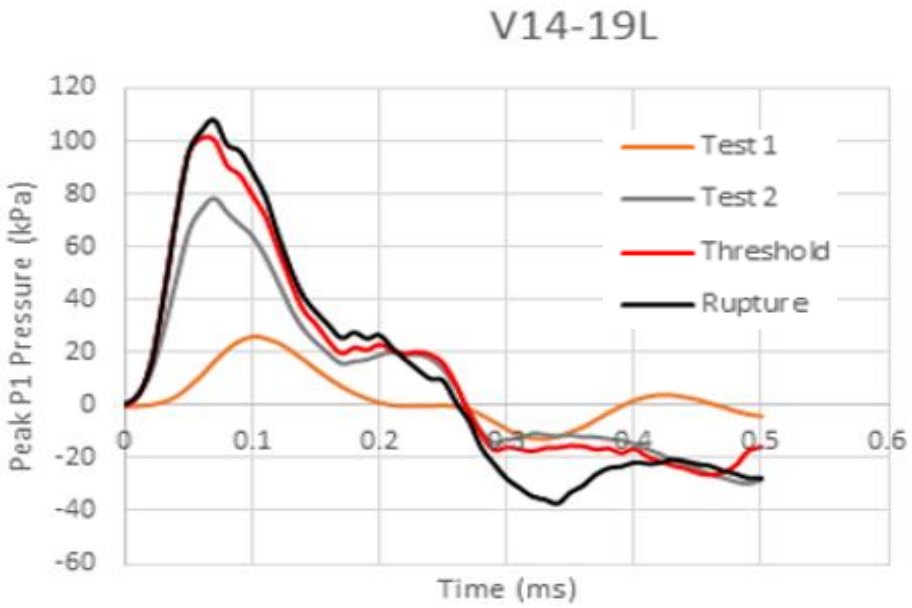

Figure 11: Resulting P1 waveforms from incrementally increasing blast experiments of temporal bone sample V14-19L.

2. A segment of the complete P1 waveform is taken to include 0.5 ms of blast waveform starting at the point of initial P1 response. The number of incrementally increased blasts ranged from three to six. No blasts after rupture occurred.
3. Each 0.5 ms duration P1 waveform was applied to the surface of the TM in ANSYS Mechanical for structure-only analyses.
4. The predicted maximum stress was plotted against the maximum exposed pressure. This was done for all increments, samples, and blast orientations. A

linear trendline, the slope of which was the stress gradient, $d\sigma_{max}/dP1$, was created for each direction.

Figure 12 shows the results of this process. The accompanying table serves to further illuminate the data and provide statistical backing for the findings.

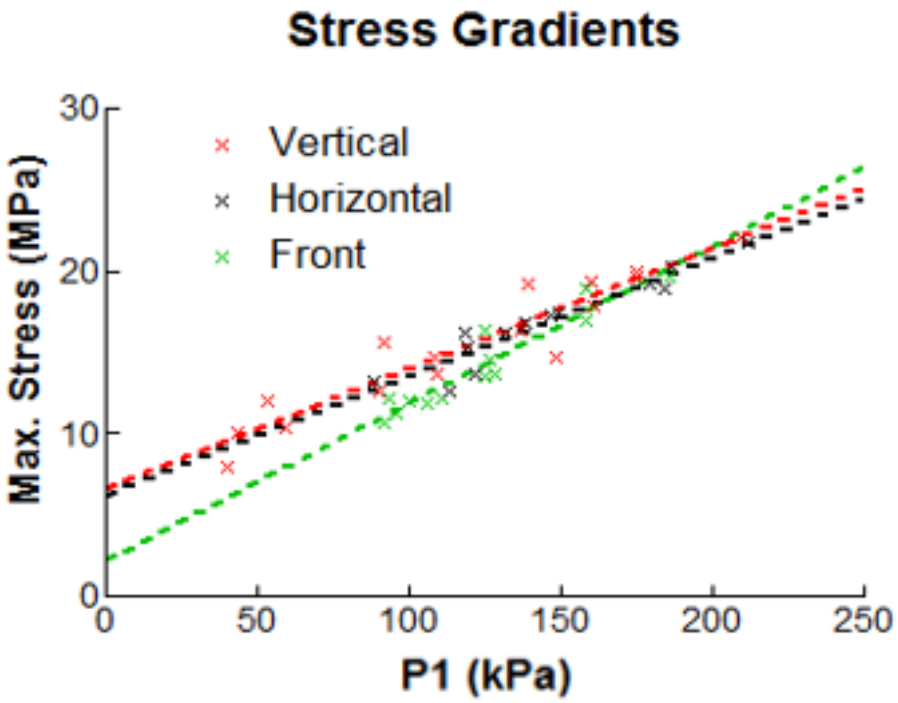

Figure 12: Maximum Stress vs. maximum P1 for the three blast orientations. Dashed line represents linear fit of the data.

Table 4: Showing the relationship between TM P1 Rupture Threshold and the predicted Stress Gradients for each blast orientation.

Direction	P1 Rupt. Thresh.	$d\sigma_{max}/dP1$	R^2
Vertical (N=4)	131 ± 23 kPa	74.1	0.89
Horizontal (N=4)	131 ± 41 kPa	73.0	0.90
Front (N=4)	112 ± 22 kPa	96.7	0.90

As can be seen in the above, the stress gradient, $d\sigma_{max}/dP1$, for the Front orientation is significantly higher than those of the Vertical and Horizontal orientations. This finding reveals that blasts in the Front orientation generate P1 waveforms that induce a greater rate of stress with respect to P1 levels than the Vertical and Horizontal orientations that induce similar rates of stress with respect to one another. This suggests that the rate of stress with respect to P1 is a more valid predictor of TM rupture than pressure level, alone.

2.4.2 Explaining Horizontal Direction P0 Rupture Threshold Level

A difficult problem arises when deciding which TM rupture threshold one ought to report; the P1 Rupture Threshold is the most straightforward since P1 is the pressure level that acts on the TM and is responsible for rupture. However, P1 levels *in vivo* are hard to obtain. The P0 Rupture Threshold is practical as it is measured external to the body, and weapons' fire pressure profiles are prevalent in literature and may be directly compared against the threshold for rupture [34] [35] [3]. An important parameter in bridging the peak pressure values, and thus rupture thresholds, of P1 and P0 is the pressure amplification ratio from P0 to P1, P1/P0. Table 3 shows that although the Vertical and Horizontal blast orientations possess the same P1 Rupture Threshold (same pressure level at the TM required to cause rupture), the Horizontal direction has a significantly lower P0 Rupture Threshold. Explaining how this occurred was achieved by providing insight into what governs P1/P0 through application of the HEM.

Four parameters were considered to impact P1/P0: canal geometry, entrance pressure magnitude, entrance velocity, and the waveform itself. A correlation study was

performed to test the effect entrance pressure magnitude had on the resulting P1/P0 value for the Vertical (N=14) and Horizontal (N=14) orientations. Figure 13 shows entrance pressure magnitude (P0) plotted against P1/P0 for the two blast orientations. The dashed line shows the linear-fit trendline. For both cases, P0 was shown to be weakly correlated with P1/P0, with R-squared (R^2) values of 0.34 and 0.11 for the Vertical and Horizontal directions, respectively. This suggests the amplification ratio is only limitedly influenced by the pressure level outside of the ear.

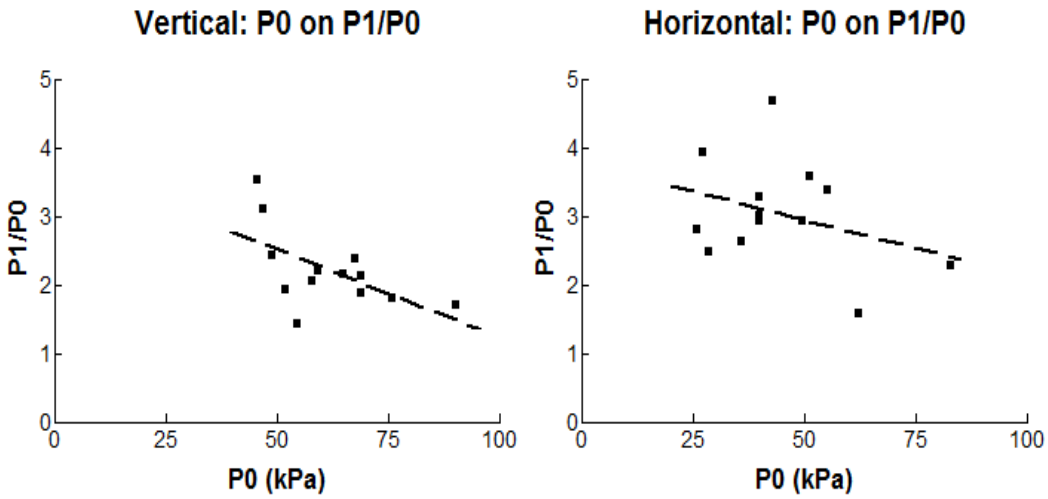

Figure 13: Showing weak correlation between entrance pressure level (P0) and resulting P1/P0 value for Vertical and Horizontal orientations.

Due to the complexity of quantifying canal geometry and waveform alterations, these parameters of P1/P0 were not studied. However, the HEM was employed to test the effect of velocity on P1/P0. In these analyses, canal geometry was controlled via the HEM ear canal and waveform effects were controlled while only altering the entrance velocity via an initialization process.

Two analyses were initiated using the P0 waveforms from the Vertical and Horizontal experimental data shown in Figure 9. The analysis duration was set to 1 ms so as to be sufficiently long to capture the initial response of the P1 waveform. Fluent does not provide the capability of prescribing both pressure and velocity at a single subsonic inlet due to restrictions of the governing equations and instead automatically calculates the velocity at the ear canal entrance based on the input pressure waveform. In the previous validation analyses, the 3-D canal domain was initialized at rest (0 Pa and 0 m/s) throughout. The entrance of the canal (a 2-D boundary) introduced pressure and velocity to the system but with zero momentum; the boundary velocity was passed onto the adjacent 3-D cells which then developed momentum based on the velocity magnitude and mass of air. Velocity cannot be prescribed or controlled while applying a pressure waveform at the canal entrance; however, through domain modification, the entrance of the ear canal may be initialized and patched with the desired velocity. The ear canal therefore was modified and split into two domains using HyperMesh as shown in Figure 14. Splitting the canal into two domains allowed for the bulk of the ear canal to be initialized at 0 Pa and 0 m/s, as before. The small fluid domain near the canal entrance was then patched with a higher velocity, as shown with red arrows in the figure below. Initializing the 3-D cells near the entrance of the canal with velocity, instead of just the 2-D cells of the canal entrance boundary, provided the system with initial momentum that more accurately models the physics of the blast wave entering the ear canal.

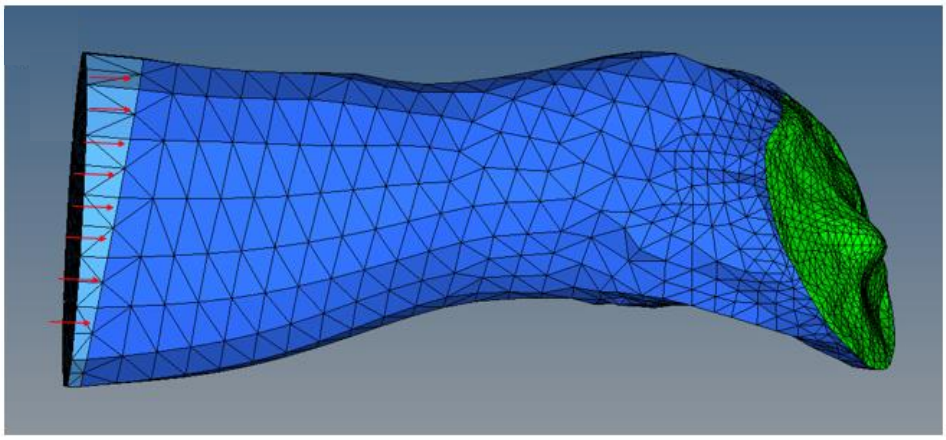

Figure 14: Modified ear canal in HyperMesh. Shades of blue represents separate fluid domains. Green boundary indicates lateral TM fluid-structure interface.

Using this new initialization methodology and the Vertical and Horizontal experimental P0 waveforms discussed in Section 2.3, two full FSI analyses were conducted to examine the P1/P0 ratio under higher initial velocity conditions. The findings are detailed below. Table 5 compares the P1/P0, entrance velocity (deemed V0), and the velocity at P1 (deemed V1) for the low, automatically calculated velocity and the modified high velocity methods for each of the examined blast orientations. All data in this table was predicted by the HEM.

Table 5: Showing velocity effect's on P1/P0 when the modified ear canal and initialization method is implemented.

Analysis	V0 (m/s)	V1 (m/s)	P1/P0
Vertical – low velocity	115	95	1.78
Vertical – high velocity	230	140	2.50
Horizontal – low velocity	105	82	1.89
Horizontal – high velocity	207	115	2.72

The same P0 waveform was applied to the entrance of the canal for the low velocity and high velocity cases for Vertical and Horizontal orientation. Through increasing only the initial entrance velocity, a significant increase is seen in P1/P0 value. In comparing the low velocity and high velocity analyses of the Vertical orientation, a 100% increase in V0 magnitude yielded a 47% increase in V1 and a 40% increase in P1/P0; for the Horizontal direction, a 97% increase in V0 magnitude yielded a 40% and 44% increase of V1 and P1/P0, respectively. This set of analyses demonstrate the effect heightened entrance velocities have on the resulting pressure amplification ratio, P1/P0. This finding suggests that the Horizontal orientation's low P0 Rupture Threshold, which is explained by its high P1/P0 value, is due in large part to increased entrance velocity when compared to the Vertical and Front orientations. The reason for the heightened entrance velocity in the Horizontal orientation is intuitive – the blast flow direction is parallel to the ear canal, i.e. the pressure front need not make a 90° turn to enter the ear canal as in the Vertical and Front orientations.

As mentioned in Section 2.3, the HEM did the worst job in predicting the P1 waveform for the Horizontal direction. The velocity magnitude Fluent automatically calculates based off of the applied pressure waveform at the canal entrance more accurately predicts the velocity of the Vertical and Front directions. The modified, or high velocity, initialization method was used to more accurately predict the P1 waveform of the Horizontal direction by more accurately modeling the entrance velocity. Figure 15 shows 1 ms of the Horizontal direction's experimental P1, low velocity P1, and high velocity P1 waveforms.

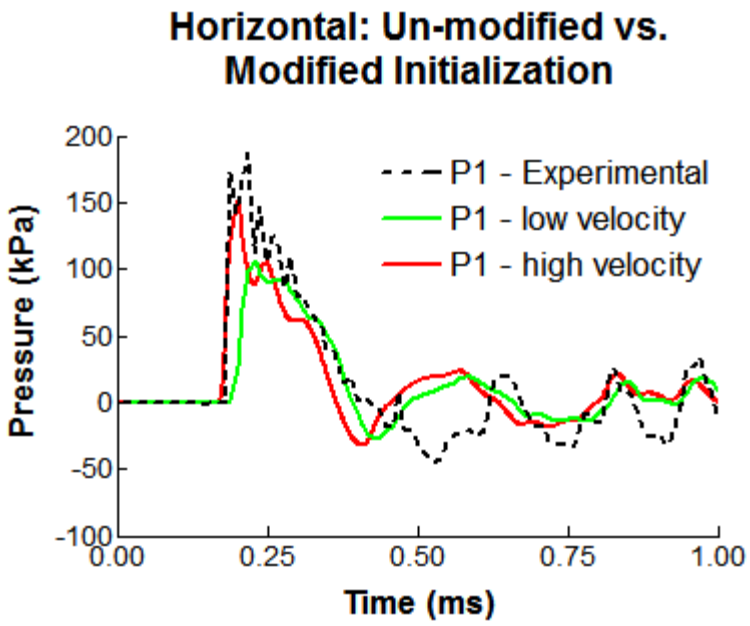

Figure 15: Un-modified vs. modified initialization results. Shows modified method results in better P1 prediction or Horizontal orientation.

As shown in the figure above, increasing the entrance velocity results in larger P1 response and a more accurate P1 prediction for the Horizontal orientation.

2.5 Chapter Summary

ANSYS Workbench was used to bridge the FE solver, ANSYS Mechanical, and the CFD solver, Fluent, for strongly coupled FSI analyses using the Human Ear Model. High-intensity pressure propagation analyses were conducted using experimental blast data as input, and then the model and analysis method was validated through comparison of the predicted pressure waveforms to the experimentally measured waveforms.

The experimental data showed that the Front orientation's P1 Rupture Threshold was uncharacteristic of the set of rupture thresholds. Through structure-only analyses this trend was explained as being caused by the high rate of stress on the TM with respect to

P1 levels the Front orientation imparts in comparison to the rates of stress of the Vertical and Horizontal directions. The experimental data also showed that the Horizontal direction had an uncharacteristically low P0 Rupture Threshold. Statistical and FSI analysis methods were taken that demonstrated the low rupture threshold of the Horizontal direction was due to the high entrance velocity that is an intrinsic phenomenon of the Horizontal orientation.

In summary, a new analysis method was introduced and the first-ever coupled analyses for blast propagation were conducted in a FE model of the human ear.

Chapter 3: Conceptual Finite Element Model for Initial Earplug Analyses under Blast Impulse

With successful validation and implementation of the HEM, the model was to be employed in the investigation of HPD behavior under blast conditions. Before HPDs were created in the HEM, it was necessary to understand the function and importance of certain EP parameters. Such parameters included the EP material properties, EP insertion depth, and a host of geometric considerations. The construction of many FE models were necessary to conduct a sufficient parametric study; altering the HEM in HyperMesh would have been an infeasible approach for such a task. Therefore, the geometric creation capabilities of ANSYS Workbench's DesignModeler was employed to create a conceptual model that could be easily altered to examine a variety of EP parameters. The unoccluded (no EP) conceptual model geometry is shown in Figure 16.

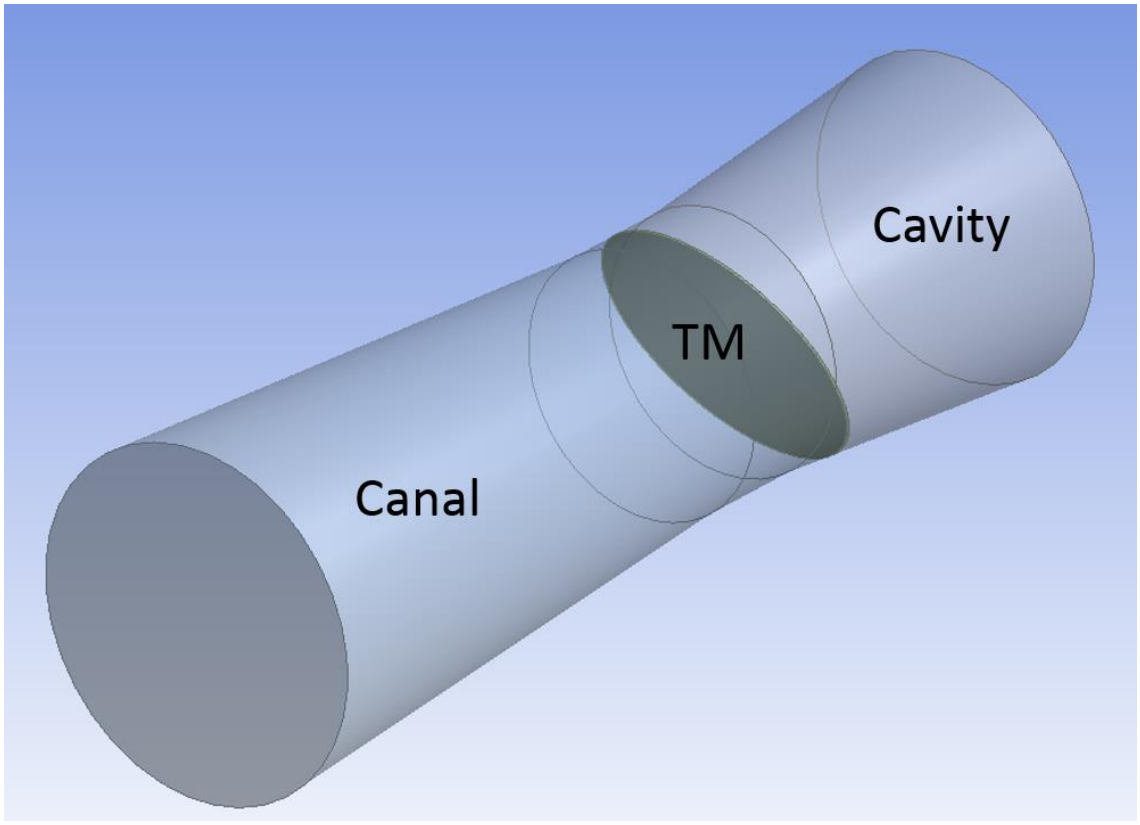

Figure 16: Unoccluded conceptual model of the human ear.

This tapered cylindrical model of the ear canal, TM, and ME cavity was created to represent the dimensions of the HEM. The diameter of the ear canal decreased from 12 mm at the canal entrance to 8 mm near the TM. The ear canal length was 30 mm. The ear canal and ME cavity was separated by a flat TM. To validate the conceptual model as a sufficient representation of the HEM, the conceptual model and HEM were subjected to identical 10 kPa triangular pressure waveforms at the entrance of the canal. The conceptual model featured linear viscoelastic material properties of the TM and two FSIs. The walls of the ear canal and ME cavity were defined as no-slip walls, as in the HEM analyses. As discussed in prior chapters, the analyses' prediction of the P1 waveform is paramount; therefore, the validation criteria of the conceptual model was that it predicted

a P1 level within 10% of the HEM's prediction. The conceptual model predicted a P1 level well within that range, and the conceptual and HEM's predicted P1 waveform comparison are compared in Figure 17.

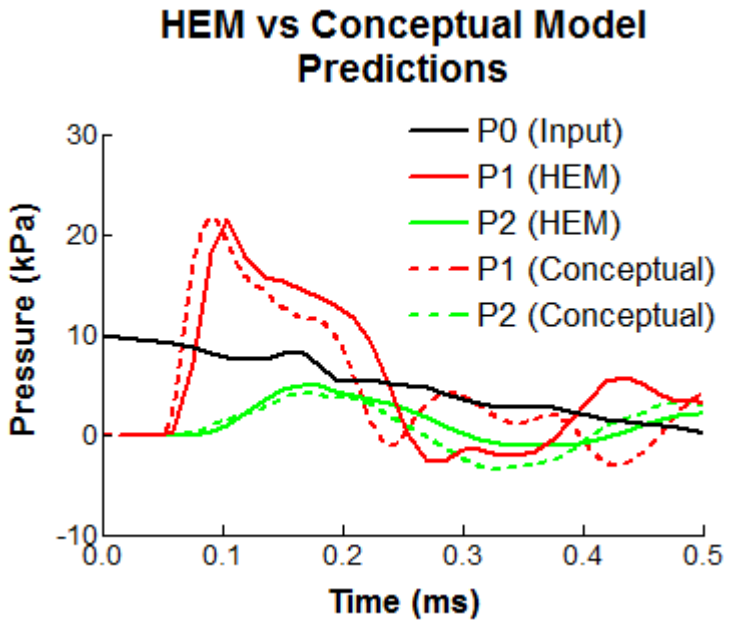

Figure 17: HEM vs Conceptual Model P1 and P2 Predictions.

The predicted waveforms of the two models were deemed, through qualitative measures, sufficiently similar, as were the P2 levels and waveforms. The conceptual model was found to be well suited for estimating the HEM's predictions and thus was implemented in the EP parametric study.

Two types of EPs fit into the scope of this study. Those were the classic foam EPs and the nonlinear EP produced by CA which featured a variable orifice and silicon triple-dome structure. Another nonlinear EP, the BP EP, was examined during experimentation and is mentioned during the parametric study, however it was not a focus of this thesis. The two considered EPs are pictured in Figure 18.

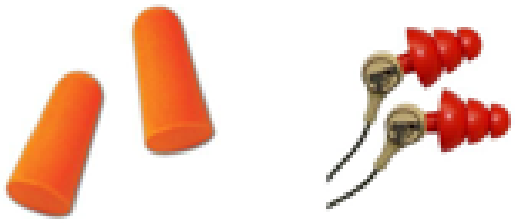

Figure 18: (Left) Classic foam earplugs. (Right) Combat Arms Earplugs.

The conceptual model was used to determine the foam material properties to be used in the analyses, understand the effect of the material properties parameters, and resolve the important parameters governing the CA EP's orifice function.

3.1 Earplug Material Properties

Determining proper EP material properties to be used in the blast analyses is necessary to predict the proper attenuation provided by the EPs. Silicon EP material properties are largely available and relatively uniform as found in literature of EP attenuation predicted by FE analysis of low-pressure harmonic analyses [13] [14] [18] [15] in contrast with material properties of foam EPs, which are less investigated [36]. Additionally, unlike silicon, the foams used in EPs are very porous and exhibit a capacity for a great deal of compressibility (at least up to 30% [36]); it is likely that the foam EP attenuation and general behavior alters under high strain rate, high-intensity pressure conditions as compared to foam behavior under harmonic, hearing-level pressure loading. Therefore, the conceptual model was utilized to determine satisfactory foam EP material properties under blast conditions.

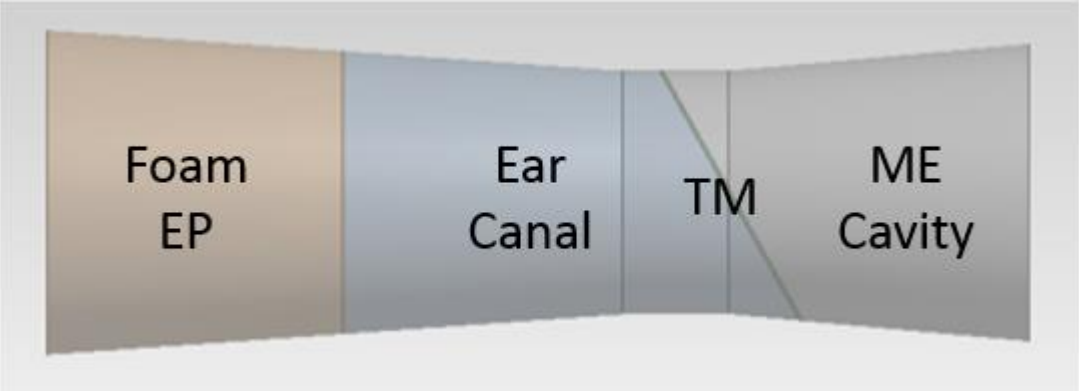

Figure 19: Conceptual model used to determine foam EP material properties.

The conceptual model ear canal was split at a distance of 11.3 mm, a distance chosen to mimic the average EP insertion depth used in FE analyses of 15 ear canal geometries [18], and divided into the foam EP and now smaller ear canal fluid domain as shown in Figure 19. The strongly coupled FSI analysis method used to validate the conceptual model was modified to include the foam EP. The foam EP was fixed along the periphery and additional fluid-structure interfaces were prescribed on the foam EP and ear canal coincident faces in ANSYS Mechanical and Fluent, respectively. A 10 kPa triangular pressure waveform with an overpressure duration of 0.5 ms was applied to the entrance of the canal onto the EP structure. A range of foam EP material properties were then examined and are shown in Table 6. These material properties were proposed by James [36] and were later adapted for use in simple FE models of EP attenuation by Sgard *et. al.* [13-18]. Both groups modeled foam EPs as isotropic solids; James included viscoelastic properties as measured during his experiments, and Sgard *et. al.* represented James' viscoelastic material behavior by including loss factor (a ratio of the viscous and elastic response of viscoelastic materials) in a linear elastic material model.

ANSYS Mechanical does not provide the capability of modeling porous solids, such as the foam found in EPs; nor was there applicable data available in literature to facilitate the application of a hyperelastic material model. Therefore, the foam EP was assumed to be an elastic solid as in previous studies. Loss factor η, is a damping parameter that may be added to a material model and is used to characterize viscoelastic response. Including the loss factor in these analyses, regardless of which material property set was used, consistently resulted in unfavorable P1 levels; therefore loss factor was not included in the foam material model.

Table 6: Foam EP Material Sets Considered for HEM Applications.

Parameter	Set 1	Set 2	Set 3
E	22.2 kPa	0.10 MPa	0.45 MPa
ρ	228 kg/m^3	220 kg/m^3	220 kg/m^3

Cadaver ear blast experiments in which the ear canal was occluded by a classic foam EP, resulted in an average P1/P0 value across P0 pressure levels of approximately 0.4. The foam material properties that resulted in the most favorable P1/P0 ratio were used for the remainder of this study. It was found that the foam material property Set 1 predicted a P1/P0 value nearest to 0.4 (0.35). It should be noted that due to the low Young's Modulus of this material property set and the large EP deformation (nearly 3 mm under 10 kPa triangular pressure waveform loading), it was recognized at this point in the study that element deformation complications were likely to be encountered as the P0 pressure intensity was increased.

Using the selected material properties as a baseline, various material parameters were increased and decreased to examine their effect on P1 level and the resulting waveform due to a 1 kPa triangular pressure waveform introduced at P0. Figure 20 below shows the effect altered Young's modulus and density material parameters have on maximum P1 response.

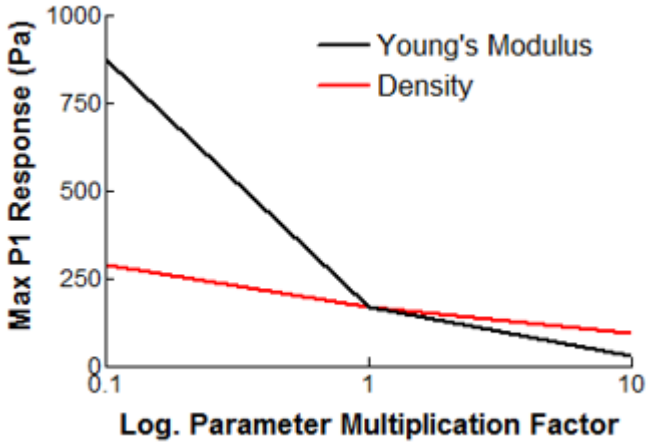

Figure 20: Foam EP Material Effect under 1 kPa Impulse.

In these studies, it was determined that the most sensitive material parameter is Young's modulus. If a more stiff foam material is assumed, a decrease in P1 level is observed, although P1 respond response time (time between peak P0 and P1 response) to the impulse pressure is quicker. A more dense foam material will decrease both P1 level and response time. Poisson's ratios ranging from 0.049 to 0.49 were prescribed to the EP and the resulting P1 waveforms were monitored. Significant change in P1 level and waveform was not detected for values of 0.049 through 0.3; at values greater than 0.4, P1 level began to decrease significantly while P1 response time was shortened. Although this group of analyses demonstrated the effect of linear elastic material parameters on P1, the defining material parameter of foam was not able to be examined – porosity.

Therefore, an analysis method capable of investigating foam's porosity effects will be necessary for more accurate foam material response. Additionally, future studies will need to be conducted that determine the way in which foam material response differs between hearing-level harmonic loading and blast impulse loading.

3.2 Examining Geometric Considerations

The function of linear EPs is very well documented in literature [3] [13] [36]; these EPs provide a high level of protection regardless of noise level (impulse or harmonic) and frequency content. Nonlinear EPs are characterized by a small orifice whose function is to exploit the acoustic impedance of impulse noise while minimally effecting the transmission of hearing-level harmonic noise. The result is an EP that mitigates hazardous noise (like the impulse noise from weapons fire) while inappreciably interfering with harmonic noise necessary for communication [37]. These EPs have been shown to provide more protection as the introduced noise level increases, hence "nonlinear" [3]. No papers have been found that examine the effects of different orifice geometries under blast conditions; such information is necessary to optimize nonlinear EPs.

The CA EP is comprised of two parts (pictured in Figure 21): the silicon triple-dome structure, whose primary function is to occlude the ear canal; and the HPC, which provides the mechanism for opening and closing the orifice that exists in the center of both parts. The HPC extends about 10 mm into the triple-dome structure, terminating at the apex of the 3rd dome (numbered right to left), and is assumed to be constructed of hard

polyethylene plastic. The remainder of the orifice (between the apices of the 1st and 3rd dome) is purely silicon in structure and features a constant 2.1 mm diameter.

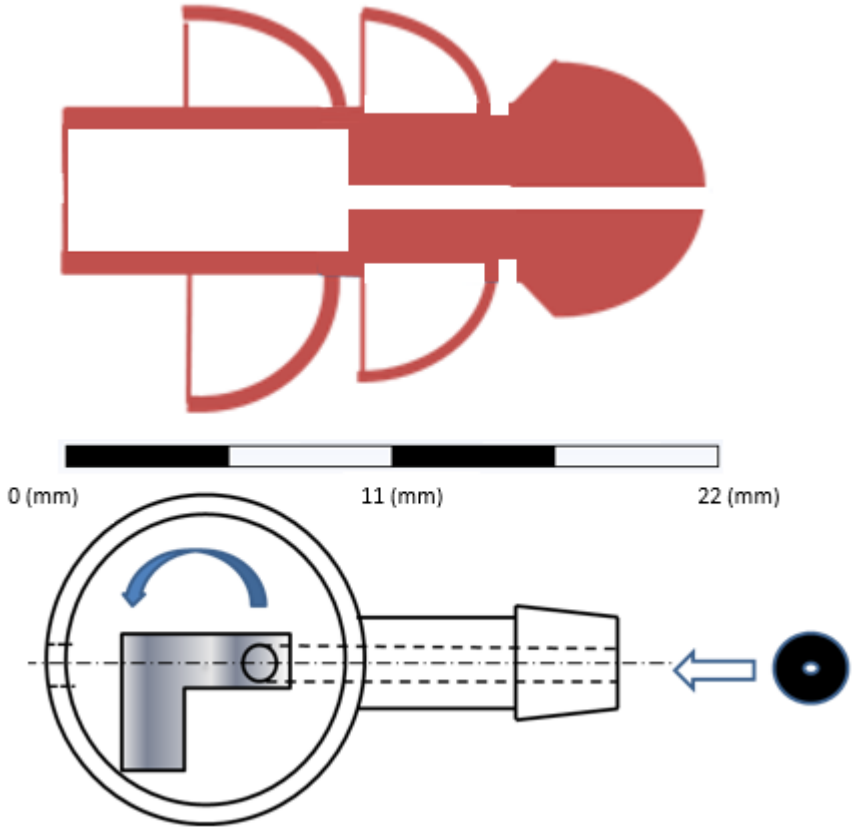

Figure 21: Schematic of the Combat Arms Earplugs. (Top) silicon triple-dome structure. (Bottom) Hard Plastic Core. Blue arrow indicates turn direction to close orifice.

It is not reported in literature how the orifice geometry (namely that of the HPC) effects the resulting P1 waveform. To determine which orifice geometric parameters most govern P1 response, the polyethylene HPC was imbedded into the foam EP of the conceptual model and strongly coupled FSI analyses were initialized with alterations made to the HPC geometry. The analyses were driven by 10 kPa triangular waveforms applied to the foam EP at the ear canal entrance and at the inlet of the orifice. As a base model, a 2.3 mm diameter straight orifice of was inserted into the foam EP. Geometry

modifications were then made to that initial orifice geometry. Preliminary analyses found that expanding a portion of the orifice in the radial direction had no impact on the resulting P1 waveform. It was also found that altering the length of expanded (and contracted) portions of the orifice from 0.5 mm to 5 mm did not significantly alter P1. Therefore, the reported parametric study examined the effects of EP insertion depth and the location and diameter of HPC orifice contraction. An overview of the geometries and parameters to be tested may be seen in Table 7. Unlike the CA HPC orifice, that of the BP EP consisted of multiple orifice contractions; a geometric model was therefore created to examine this geometry. The results will be discussed in the following pages.

Table 7: HPC Parametric Study Geometries and Parameters.

Designation	Parameter Tested	Dimensions (mm)
FOAM	Insertion depth of foam EP	5.8 11.3 15
Straight	Insertion depth with constant orifice	5.8 11.3 15
Entry	Location & diameter of orifice contraction	1 0.5
Mid	Location & diameter of orifice contraction	1 0.5
End (CA)	Location & diameter of orifice contraction	1 0.5
Battleplugs	Location & diameter of orifice contraction	1 0.5

The P1 waveform was investigated for three foam EP insertion depths; these depths were 5.8, 11.3, and 15 mm as measured from the ear canal entrance and correlate to shallow, average, and deep insertion depths, respectively, of EPs found in literature

[14] [15]. It was found that greater insertion depth corresponded to a decrease in P1 level and an increase in P1 response time; this is shown graphically in Figure 22.

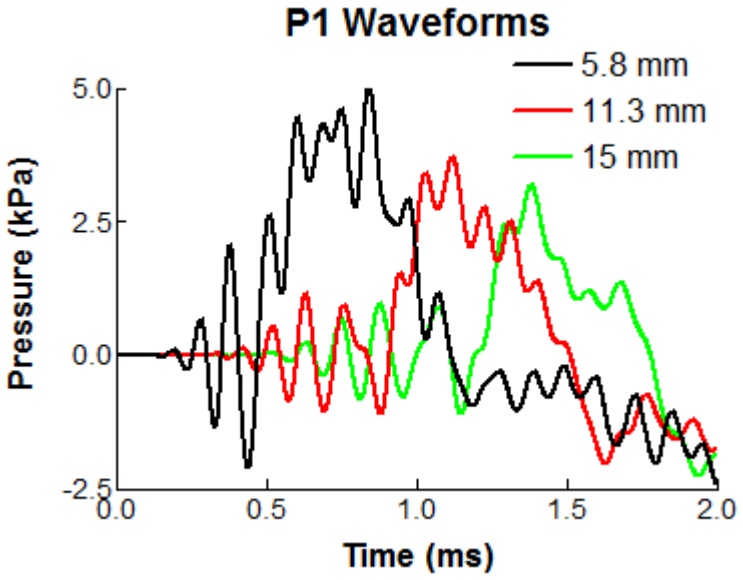

Figure 22: Foam insertion depth resulting P1 waveform comparison.

Three geometries with a constant 2.3 mm diameter orifice were created to investigate insertion depth's impact on P1 waveform resulting from ear canal occlusion by a perforated EP. Figure 23 below shows the comparison of the resulting P1 waveforms.

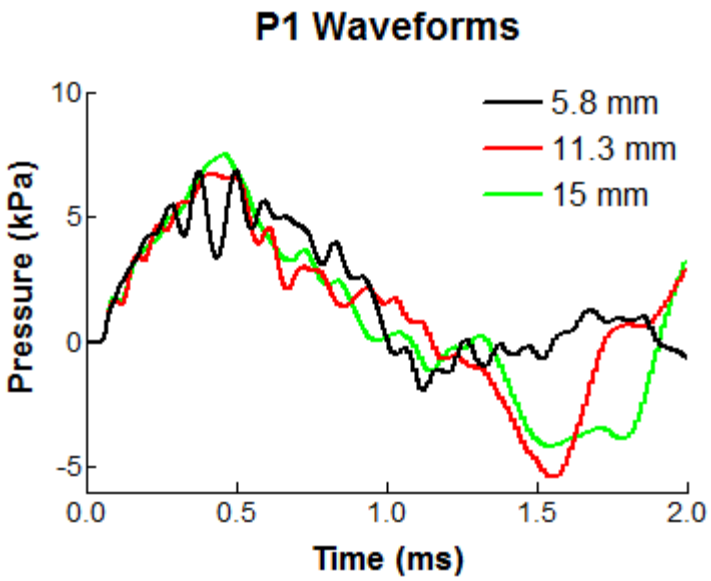

Figure 23: Straight geometry insertion depth resulting P1 waveform comparison.

Unlike the foam EP, the relationship between insertion depth and P1 level and response time is unclear; the 11.3 mm insertion depth generates the lowest P1 level of 6.7 kPa. Of note is that the 5.8 mm insertion depth results in the least amount of negative overpressure. This knowledge may prove useful when optimizing EP design, as a study in chinchillas [33] has shown that negative overpressure results in much higher stress levels as the TM is effectively pulled towards the ear canal entrance as contrasted against positive overpressure. The Straight geometry of 11.3 mm insertion depth was used as a baseline from which to modify and compare the other orifice geometries.

Three sets of geometries were created with single diameter contractions located at the entrance of the ear canal, in the middle of the EP, and at the end of the EP, designated Entry, Mid, and End, respectively. The End geometry coincides with the HPC structure of the CA EP. An additional geometry was created that estimates the HPC architecture of the BP EP, which features two orifice diameter contractions. The first

(leftmost) of the BP contractions separates staggered orifice diameters of 3.2 and 3.7 mm, left to right, as pictured in Figure 24 (4).

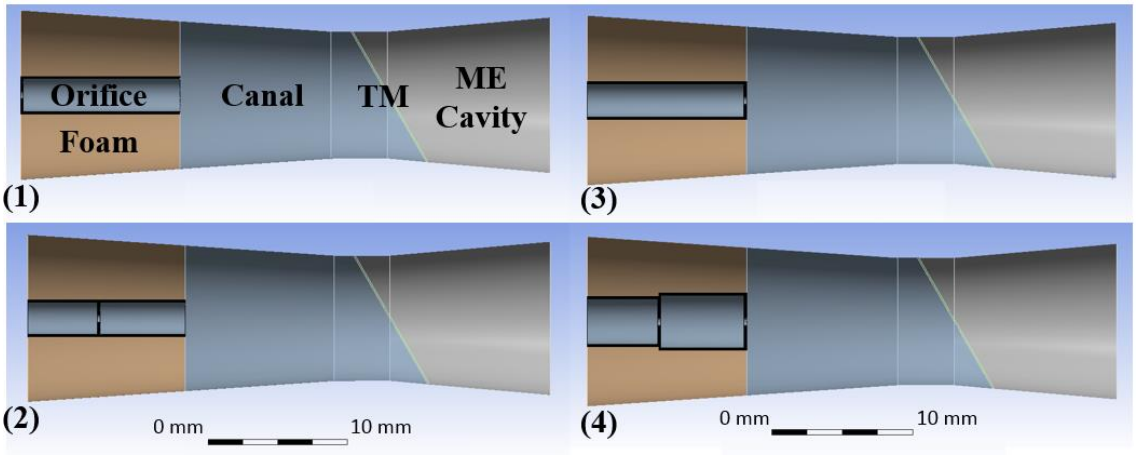

Figure 24: 0.5 mm orifice contraction geometries of (1) Entry, (2) Mid, (3) End, (4) BP.

Analyses with the aforementioned geometries were conducted with contraction diameters of 0.5 and 1.0 mm. Figure 25 show the contraction diameter effect by comparison of the resulting P1 waveforms for the Entry, Mid, End, and BP geometries, respectively.

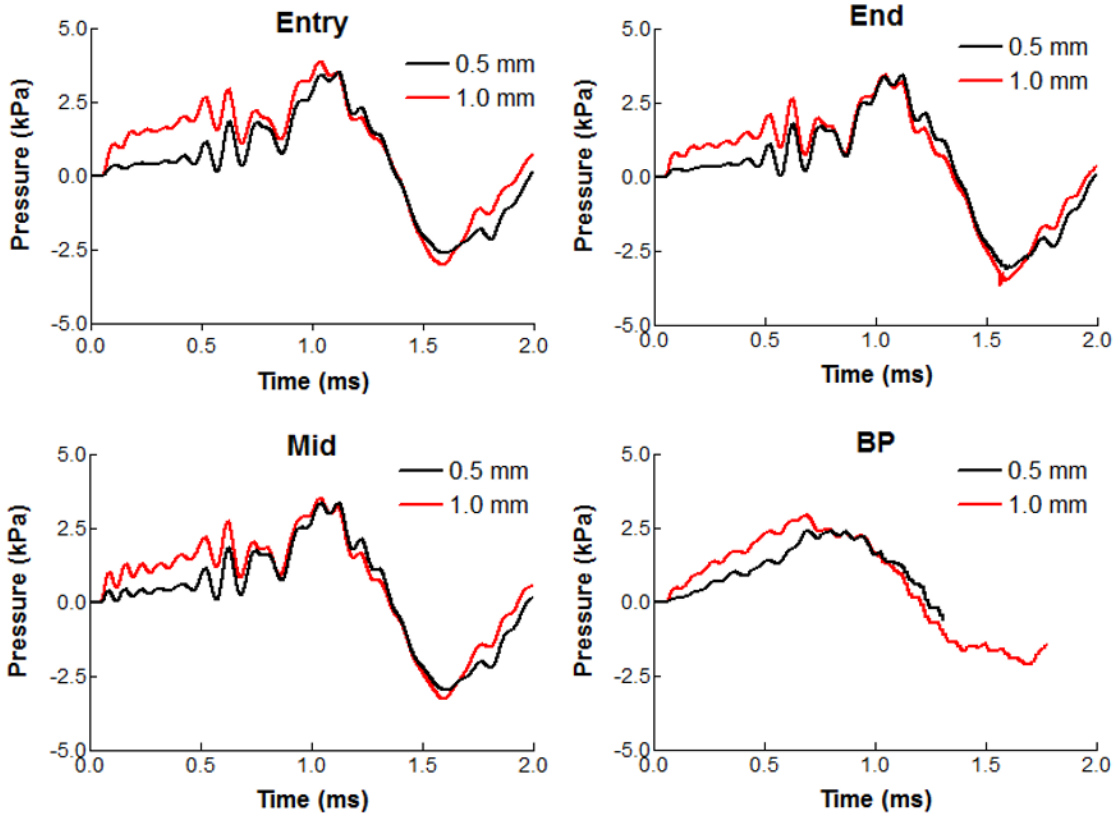

Figure 25: Comparison P1 waveforms of 0.5 and 1.0 mm orifice contraction diameters in Conceptual Ear Model.

As displayed in the plots above, decreasing the contraction diameters from 1.0 mm to 0.5 mm did not significantly alter the maximum P1 level; it did, however, result in a decrease in the area under the curve from t = 0 ms to approximately t = 0.8 ms. Additional studies on what is the major contributor to TM damage – peak P1 value or area under the curve – will need to be conducted before this finding may provide conclusions on most appropriate design.

Figure 26 and Table 8 may be used to draw conclusions on this parametric study. Figure 26 compares the P1 waveforms of the Entry, Mid, End, and BP geometries with 0.5 mm contraction diameters while contrasting them against the Straight orifice

geometry, foam EP, and unoccluded ear canal P1 waveforms. Table 8 gives the measured peak pressure values at the monitored P1 and P2 locations, the EP attenuation (pressure at the TM subtracted from the introduced pressure at the canal entrance, [P0 – P1]), and the predicted insertion loss (P1 level of unoccluded ear minus P1 level with EP).

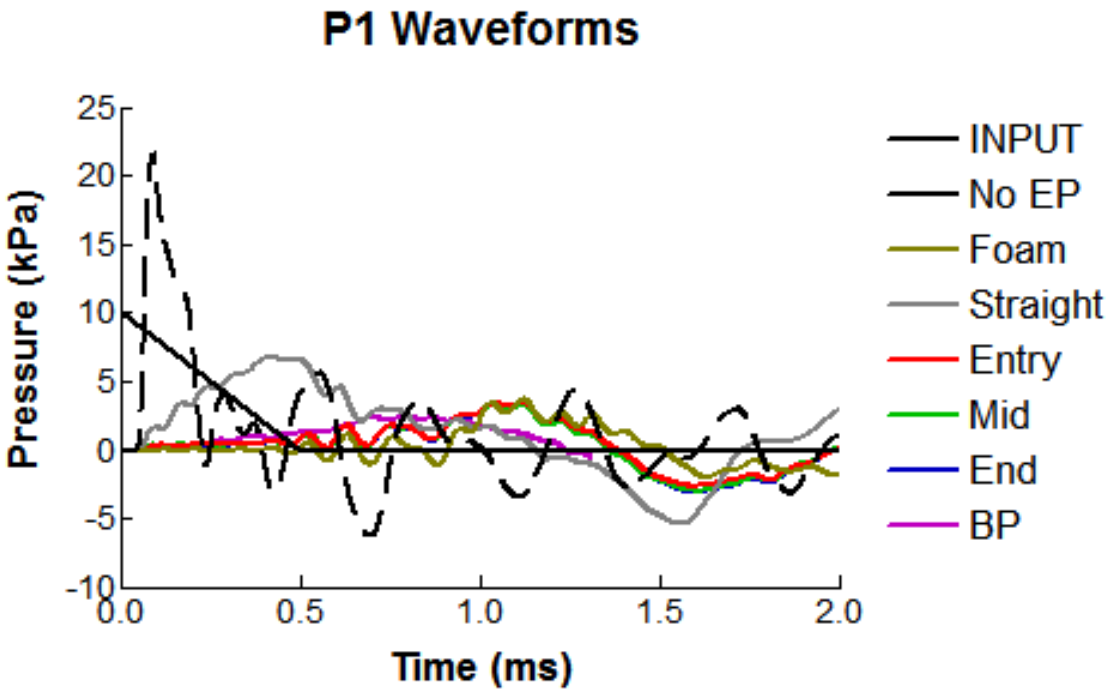

Figure 26: Comparing 0.5 mm diameter orifice contractions with the input, unoccluded, foam, and constant diameter cases.

Table 8: Compilation of conceptual model predicted pressure values and EP attenuation and Insertion Loss.

Geometry	P1 (kPa)	P1 (dB)	P2 (kPa)	Atten. (dB)	IL (dB)
Foam 5.8	5.0	168	2.4	6.0	13
11.3	3.7	165	2.1	8.6	15
15	3.2	164	1.8	9.9	17
Straight 5.8	6.9	171	2.7	3.3	10
11.3	6.7	171	2.5	3.5	10
15	7.5	172	2.5	2.5	9
Entry 0.5	3.4	165	1.6	9	16
1.0	3.8	166	1.7	8	15
Mid 0.5	3.4	165	1.7	10	16
1.0	3.5	165	1.6	9	16
End 0.5	3.4	165	1.7	9	16
1.0	3.4	165	1.6	9	16
BP 0.5	2.4	162	1.3	12	19
1.0	2.9	163	1.5	11	17

This study illuminated the relationship between basic EP geometric configurations and the resulting pressure waveforms monitored near the TM. The findings are summarized below.

- For foam EP without orifice, a greater insertion depth results in greater pressure level attenuation at P1; foam EP with constant diameter HPC does not show the same trend, with the greatest insertion depth resulting in the highest pressure.
- The HPC orifice contraction diameter does not significantly alter the peak P1 level, although a larger diameter does result in more area under the curve during the first millisecond.
- A single orifice contraction, regardless of location, will result in nearly identical waveforms as measured at P1 (shown by overlapping waveforms in Figure 26).
- Multiple orifice contractions (as in the BP case) provide greater attenuation as measured at P1 than single contraction orifices.
- Note: although analyses with HPC inserted into foam EP do not model either of the investigated NL EPs accurately, this study is applicable for comparative purposes.
- Hearing-level harmonic testing is still necessary to accurately characterize HPC orifice function.

Chapter 4: Human Ear Model to Predict Earplug Attenuation under Blast Conditions

Currently, the only computational approach that is capable of successfully predicting linear and nonlinear EP attenuation and inner ear response due to high-intensity pressure impulse is the AHAAH model created by the Army Research Laboratory. As with the HEM, AHAAH analyses may be driven by experimentally measured waveforms. The most notable limitation of the AHAAH model, however, is its inability to assess pressure profile throughout the ear canal and the stress distributions imparted on the tympanic membrane (TM). The FEM coupled with CFD allows for the deduction of fluid pressure propagation and the development of velocity streamlines with respect to time, as well as stress concentrations developed in the structure caused during FSI.

This chapter aims to describe the newly created HEM to predict linear and nonlinear NL EP attenuation during mid- and high-level impulse blast conditions. The 3-D meshes of the two EPs were created to occlude the ear canal and the ear canal was modified to more closely resemble those found in Sgard's work [18]. Strongly coupled FSI analyses were conducted that were driven by experimentally measured P0 waveforms (located near the ear canal entrance) ranging from 14 – 40 kPa. The predicted waveforms were compared against experimental waveforms; the comparisons are discussed and future improvements to the model are examined.

4.1 Generating Meshes

For this preliminary set of EP analyses, the construction of three individual HEMs were required to represent the cases of the unoccluded ear canal and ear canal occlusion

via the foam and CA EPs; HyperMesh was used for all meshing operations. To produce a model that more closely follows examples of other FE models of EPs in literature [13] [14], a layer of skin with an average thickness of 1.5 mm was added to the ear canal in the HEM referenced to in Chapter 2. In the referenced journal articles, the FE models, which terminate at the TM, also include cartilage and bone surrounding the ear canal. It may be important to include these components into the model during future studies of blast's effects on the cochlea, as it has been shown that bone conduction produces cochlear response [38]. The HEM modified to include ear canal skin was used for the unoccluded case.

Creating the foam occlusion HEM required modifying the fluid domain of the ear canal in addition to generating the structure of the foam EP (shown in Figure 27). The foam EP was modeled to completely occlude the ear canal; i.e. no leaks were present and the nodes of the foam EP and skin were coincident along the wall of the ear canal. The foam EP insertion depth as measured from the entrance of the canal to the EP's apex was 12 mm. The foam EP and the fluid of the ear canal were comprised of 711 and 8,563 elements, respectively.

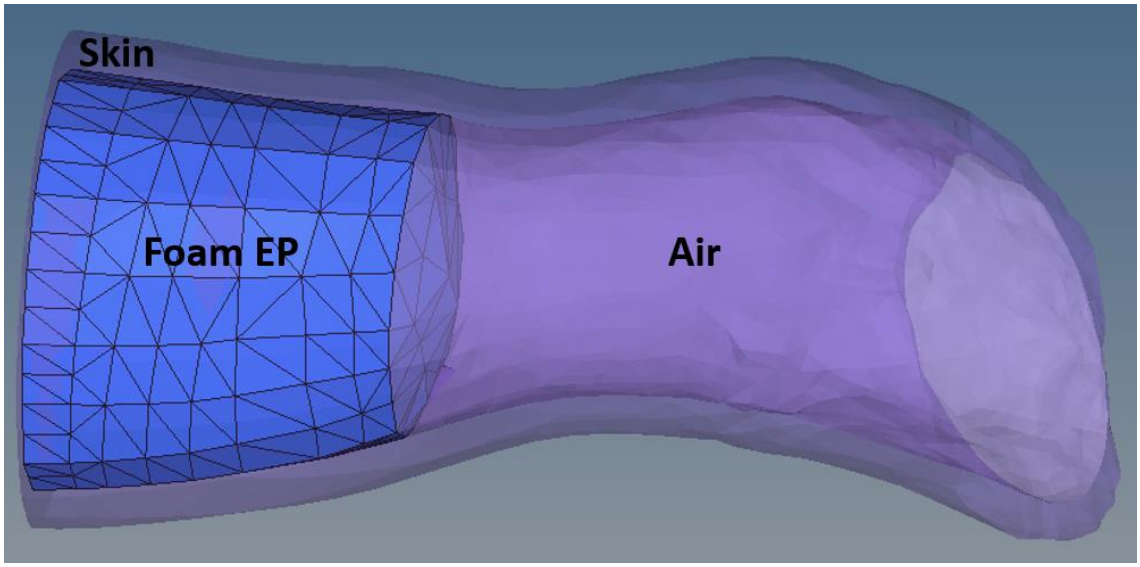

Figure 27: Ear canal modified to include foam EP and (Transparent) skin and ear canal fluid.

During experiments of the CA EP, it was observed that the third and largest dome was seldom inserted into the ear canal. In the average ear, only the first two domes are fully inserted into the ear canal, with only the apex of the third dome set inside; the primary function of the third dome is to obstruct the entrance to the ear canal (shown in Figure 28).

Figure 28: Combat Arms EP inserted into scale ear model. [Shows the third of the triple-domes blocking, but not entering the ear canal.]

As the HPC of the CA EP terminates prior to the apex of the third dome, the HPC was not included in the HEM. Thus, only the CA EP silicon triple-dome was generated within the HEM. A Vernier caliper was used to measure the dimensions of the CA EP, which are shown with respect to the resulting mesh in Figure 29. The triple-dome structure consisted of 23,440 elements – this large number is due to the small element size of the inner face of the orifice. The orifice and flanges of the triple-dome structure resulted in additional fluid volumes through and between the flanges of the CA triple-dome. The total modified ear canal fluid mesh consisted of 39409 elements.

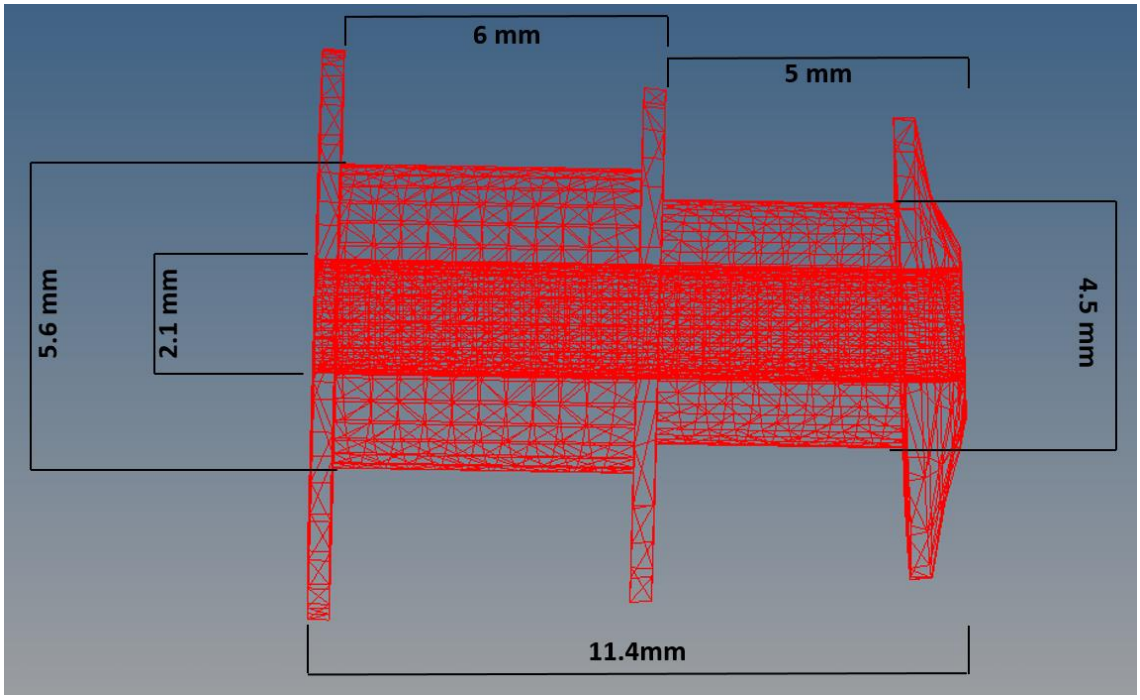

Figure 29: Wiremesh representation of Triple-dome used in HEM analyses with selected dimensions.

The three models of the unoccluded ear canal and the ear canal occluded by foam EP and CA EP triple-dome were then imported into ANSYS Workbench for strongly coupled FSI analyses.

4.2 Earplug Analysis Method

In order to discern the HEM's predictability of EP attenuation under blast conditions, the model must be prescribed appropriate material properties and boundary conditions under valid physical assumptions. Should these conditions be met, the resulting pressure waveforms as monitored at P1, just before the TM in the ear canal, and P2, inside the middle ear cavity, will closely agree with experimental data measured during cadaver ear blast studies. Waveforms from a single experimental specimen,

TB 16-30R, were used to both drive the HEM analyses and compare to the resulting predicted waveforms as a means for model verification. TB 16-30R was subjected to a battery of blasts at two blast levels – mid-level (14 – 19 kPa) and high-level (38 – 51 kPa). At each pressure level, the sample was exposed to blast overpressure while fitted the foam EP, the CA EP at maximum (closed orifice) and minimum (open orifice) protection settings, and the CA triple-dome-only before finally being blasted with an unoccluded ear canal. During blast exposure, pressure waveforms were measured at P0, near the ear canal entrance, and P1 and P2.

The analysis method for predicting P1 and P2 waveforms in the unoccluded HEM is identical to that mentioned in Chapter 2, with the exception of additional considerations due to the addition of the ear canal skin component. Material properties were extracted from Sgard's group [14] who defined skin as an elastic isotropic solid with properties of: 0.42 MPa (Young's modulus), 1050 kg/m^3 (density), 0.43 (Poisson's ratio), and 0.2 (loss factor). Material beta damping was applied to the skin to introduce loss factor, a convenient value to represent viscoelastic behavior, via Equation 10,

$$\beta = \frac{\eta}{\pi f} \tag{10}$$

where, β is the material beta damping factor, η is the loss factor, and *f* is frequency. A complication arises when prescribing beta damping in a transient analysis due to the frequency component of the damping. Therefore, the average value of beta damping was taken from 0 – 10 kHz. Additional fluid-structure interfaces were applied between the skin and fluid of the ear canal in ANSYS Mechanical and Fluent, respectively. Two analyses were initiated through application of the mid- and high-level P0 waveforms recorded from TB 16-30R unoccluded blast exposures onto the skin and fluid boundaries

at the ear canal entrance. The proceeding P1 and P2 pressure waveforms were then compared to experimental waveforms from the same exposures.

The foam EP occluded ear canal HEM (displayed in Figure 30) utilized identical material properties for foam as discussed in Chapter 3. To allow for the transfer of pressure into the fluid of the ear canal, fluid-structure interactions were defined on the EP/ear canal boundary. Experimental P0 waveforms were applied directly onto the structures of the skin and foam EP at the ear canal entrance.

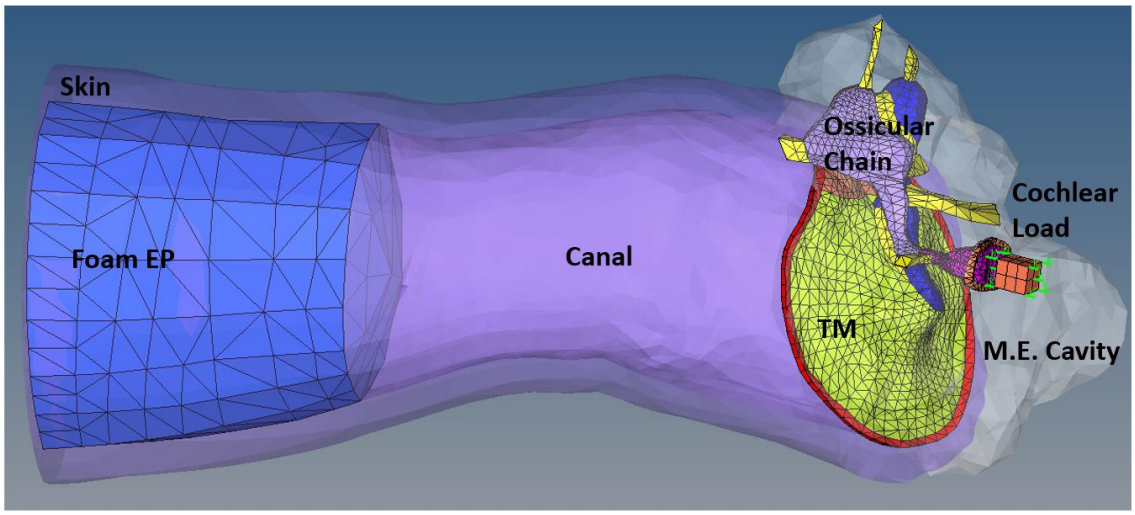

Figure 30: Complete HEM with foam EP occlusion.

Figure 31 shows the HEM with CA triple-dome occlusion. The applied silicon material properties were adapted from literature [14]. The EP was defined an elastic isotropic solid with properties: 1.2 MPa (Young's modulus) 1150 kg/m^3 (density), 0.48 (Poisson's ratio), and 0.12 (loss factor). As in the case of the ear canal skin, the loss factor was represented as the average material beta damping factor from 0 – 10 kHz. Four FSIs were applied between the EP and air in the ear canal. Since the HEM model does not include the HPC, the CA maximum and minimum protection settings exposure

waveforms were not utilized in this study. Triple-dome-only P0 blast exposure waveforms were applied to the skin and triple-dome EP at the entrance of the canal in ANSYS Mechanical; in Fluent, the identical waveforms were applied to the entrance of the EP orifice.

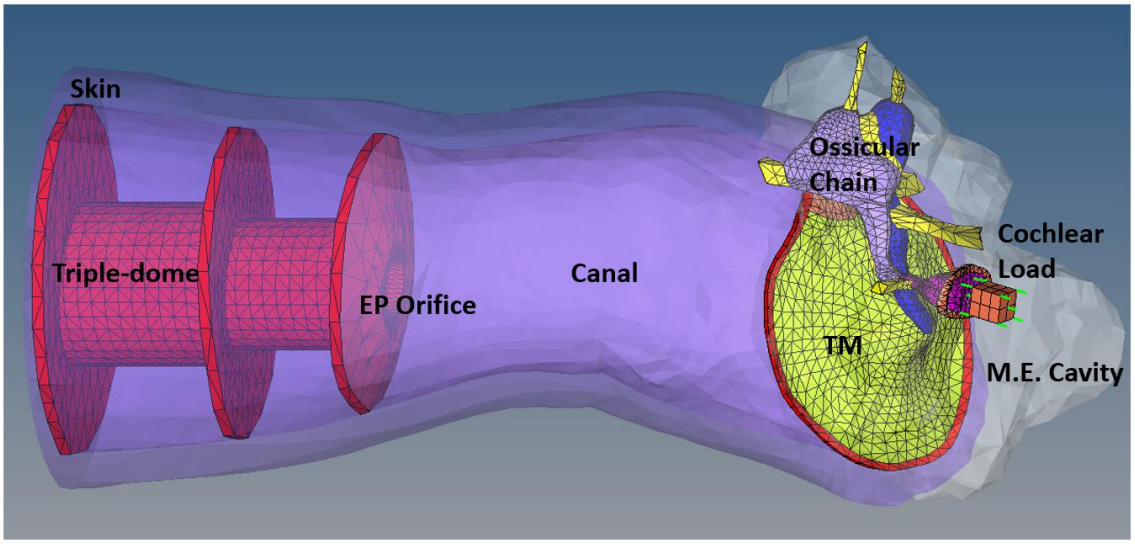

Figure 31: Complete HEM with CA triple-dome occlusion.

4.3 Results and Predicted Waveforms

There are three primary means of evaluating hearing protection devices – that is via determining P1/P0 ratio, EP attenuation, or IL. Attenuation is the measure of how much an incident pressure level outside the ear was reduced as compared to the pressure level at the TM; mathematically, EP attenuation is P1 subtracted from P0. IL is determined by subtracting the pressure level near the TM with EP inserted from the pressure level near the TM of the unoccluded ear canal. All evaluation methods are used during the comparison of the HEM predicted waveforms to the experimentally measured waveforms of sample TB 16-30R.

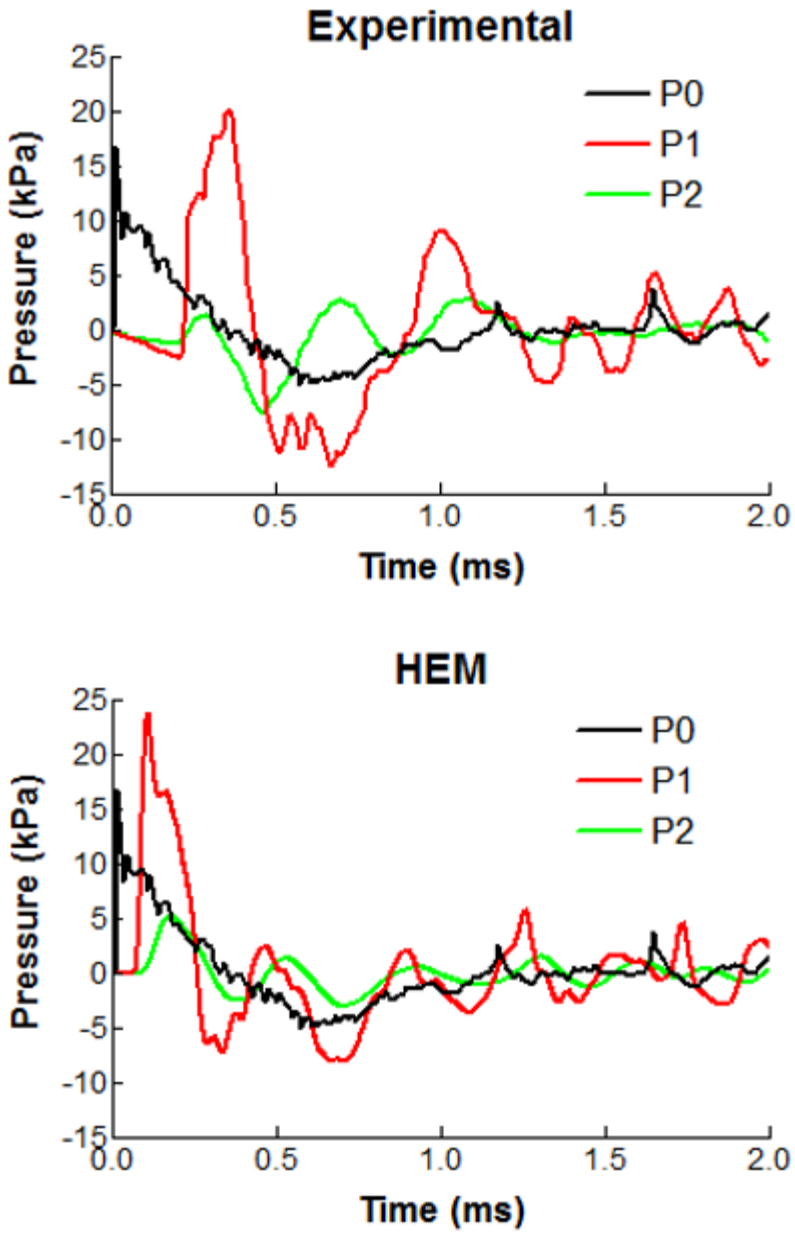

Figure 32: Unoccluded mid-level exposure experimental vs. predicted pressure profiles.

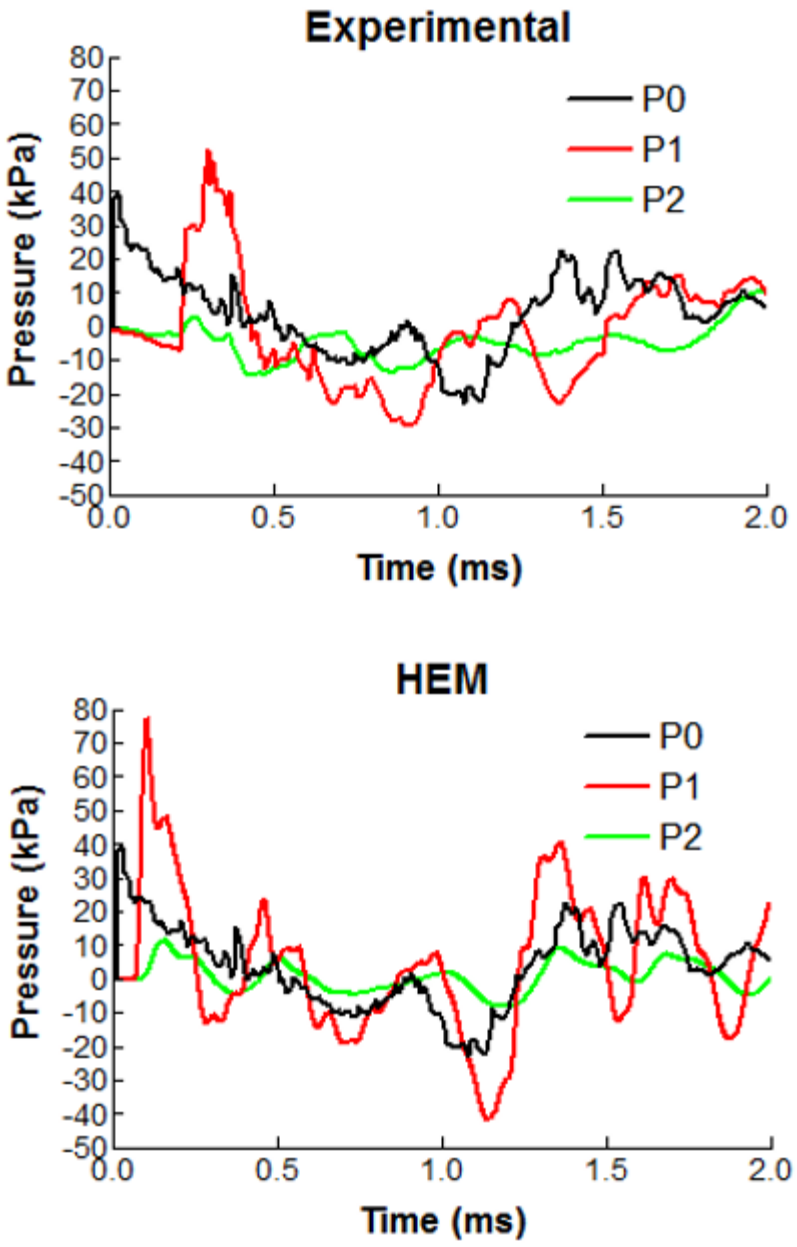

Figure 33: Unoccluded high-level exposure experimental vs. predicted pressure profiles.

Figures 32 and 33 above show 2 ms of the unoccluded ear experimental pressure waveforms compared to the HEM predicted waveforms for mid- and high-level blast exposures, respectively. The predicted P1 and P2 levels of the mid-level exposure exceeded the peak pressure values measured during experimentation; this occurrence was

more exaggerated in the case of high-level exposure. Overall, the predicted and measured P1 and P2 waveforms were in agreement. The predicted versus measured P1/P0 values were 1.4 versus 1.2 and 2.0 versus 1.3 for mid- and high-level exposures, respectively.

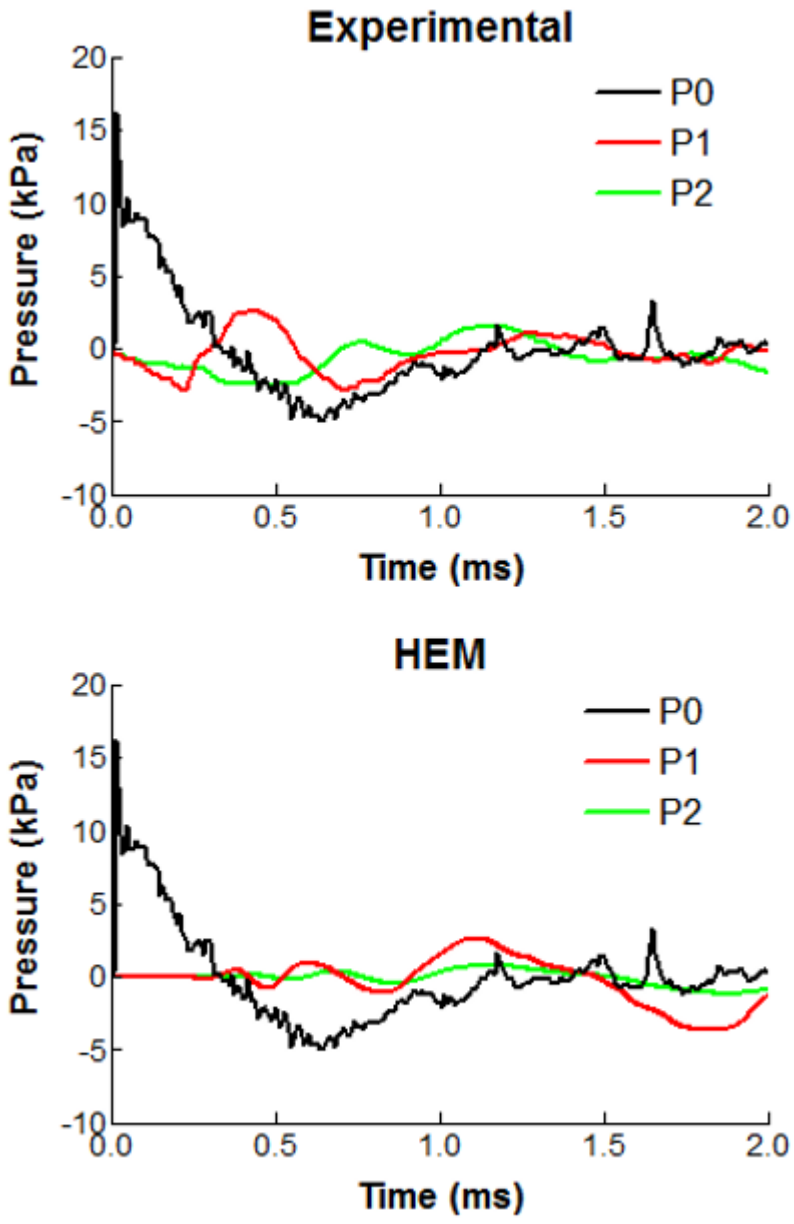

Figure 34: Foam EP occluded mid-level exposure experimental vs. predicted pressure profiles.

The waveforms of the foam EP occluded ear canal in response to mid-level blast exposure as measured via experimentation and predicted via HEM are shown in Figure 34 above. It was apparent that the HEM with foam EP occlusion and current analysis settings were insufficient to adequately predict the P1 and P2 waveforms, although both measured and predicted P1/P0 values were 0.16. Only mid-level blast exposure analysis was conducted with this model; high-level pressures distorted the foam EP to the point of analysis termination. Although the linear elastic representation of the foam EP has been implemented successfully in other studies [13] [14], this material model is unsuitable for the high pressure and high strain rate analyses inherent when modeling blast exposures. A more appropriate nonlinear material model is necessary to accurately predict the EP attenuation of foam materials subjected to blast overpressures.

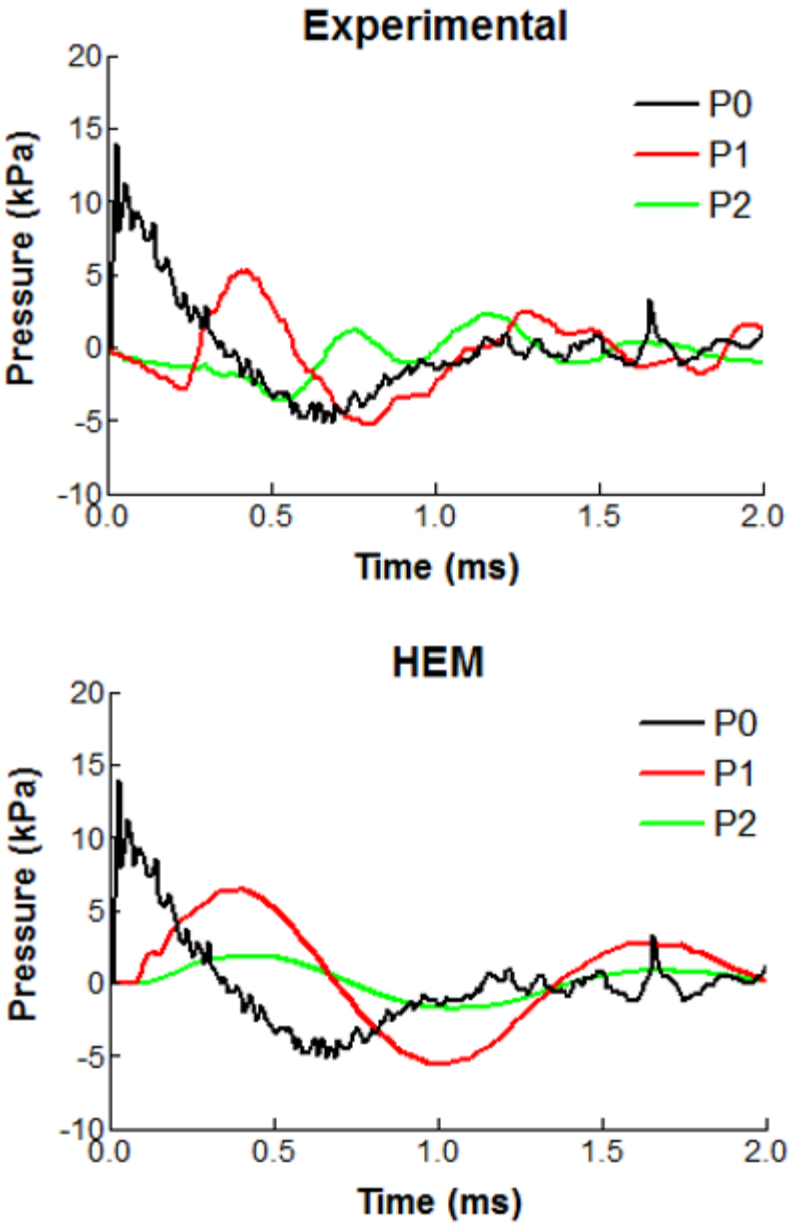

Figure 35: CA triple-dome occluded mid-level exposure experimental vs. predicted pressure profiles.

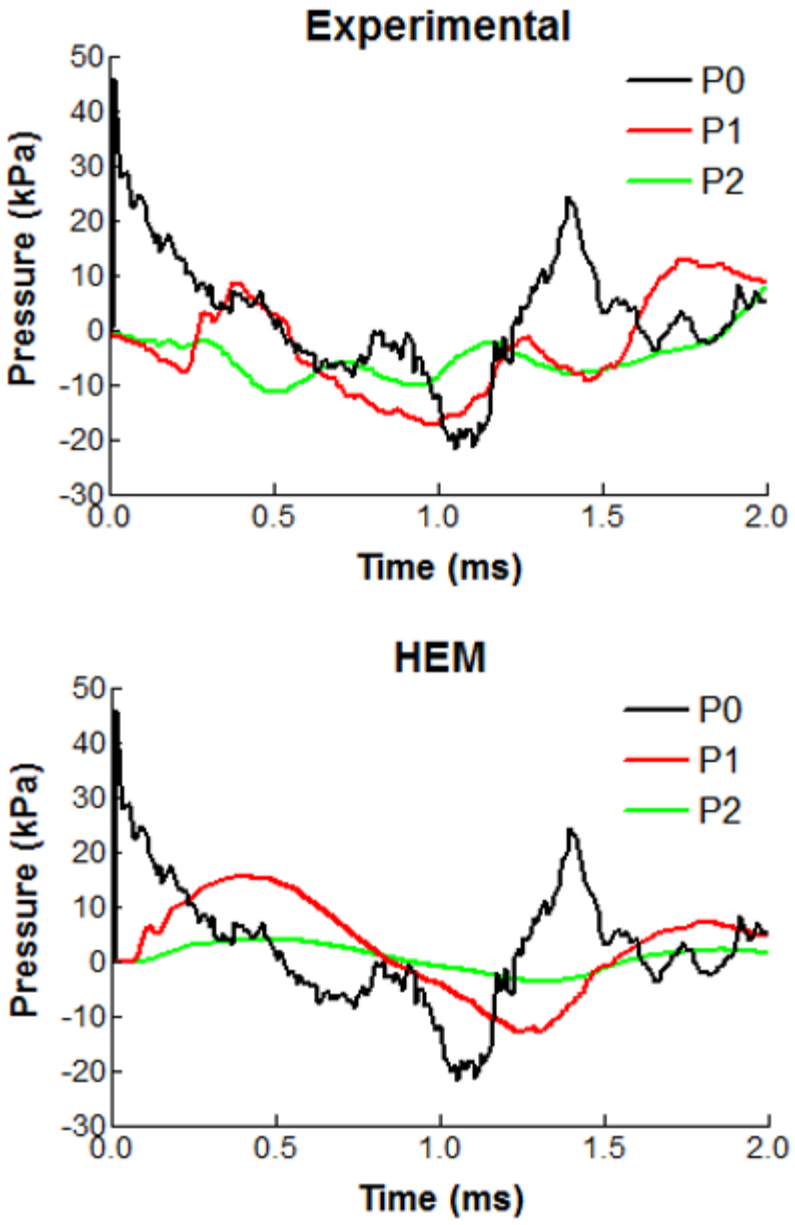

Figure 36: CA triple-dome occluded high-level exposure experimental vs. predicted pressure profiles.

Shown above (Figures 35 and 36) are the experimental and predicted pressure waveforms from mid- and high-level blast exposures of CA triple-dome-only occluded ears. The predicted waveforms generally agreed with the shape of the experimental pressure profiles; the greatest discrepancy was in the duration of positive P1 overpressure

when compared to the relatively short duration of initially positive overpressure observed in the experiment (roughly 0.25 ms). A portion of this is explained by the initial drop in pressure level measured during experimentation that is likely due to experimental setup. The experimental P1waveform also contains a higher degree of undulation than was predicted, although this may be simply due to variations in canal geometry. For mid-level exposure, predicted versus measured P1/P0 value, EP attenuation, and IL were 0.46 versus 0.39, 6.7 dB verses 8.2 dB, and 11.4 dB verses 11.3 dB, respectively. Predicted versus measured P1/P0 value, EP attenuation, and IL for high-level exposure were 0.34 versus 0.29, 9.3 dB versus 10.8 dB, and 13.9 dB versus 12.0 dB, respectively. Table 9 below consolidates the results of the analyses of the unoccluded and occluded models of the HEM.

Table 9: Consolidated representation of unoccluded and occluded HEM blast exposure results

Exposure	Waveform	P1 (kPa)	P1 (dB)	P2 (kPa)	P1/P0	Atten. (dB)	IL (dB)
Mid-level unoccluded	Exp.	20	180	2.8	1.2	-1.6	N/A
	Pred.	24	182	5.3	1.4	-3.1	N/A
High-level unoccluded	Exp.	53	188	10	1.3	-2.6	N/A
	Pred.	77	192	11	2.0	-5.9	N/A
Mid-level Foam EP	Exp.	2.6	162	1.6	0.16	16	18
	Pred.	2.6	162	0.8	0.16	16	19
Mid-level Triple-dome	Exp.	5.4	167	1.6	0.39	8	11
	Pred.	6.4	170	1.9	0.46	7	11
High-level Triple-dome	Exp.	13	176	8.0	0.29	11	12
	Pred.	16	178	4.0	0.34	9	14

The HEM was able to predict peak P1 levels (and identically P1/P0 values) within 33% (averaged), 1.2 %, and 18% (averaged) of the experimental peak values for the unoccluded, foam EP occluded, and CA triple-dome occluded ear canal cases, respectively. The CA triple-dome analyses approximated EP attenuation and IL within 16% (averaged) and 7.8% (averaged), respectively, as compared to measured values.

The HEM modified to include foam EP and CA triple-dome ear canal occlusion with strongly coupled FSI analyses conducted in Fluent/ANSYS Mechanical was capable of predicting EP function with respect to resulting pressure profiles that largely agrees with available experimental data. The CA EP maximum and minimum settings were not

examined in this study, as further modeling work must be completed to include the CA HPC in the HEM.

As an example of the possible utility of the HEM to aid in nonlinear EP design, consider Figure 37.

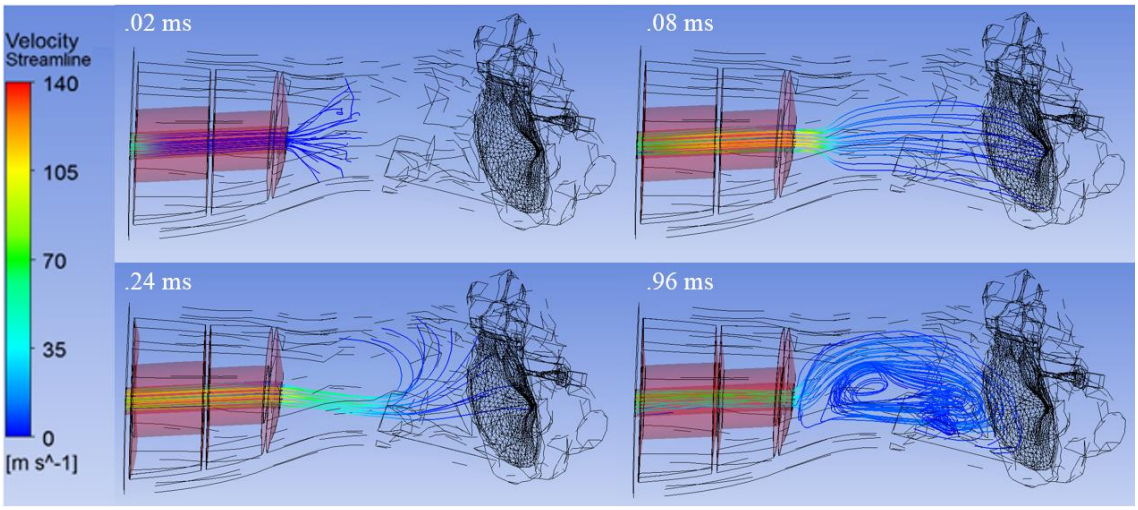

Figure 37: Time history of velocity with streamlines in CA triple-dome occluded HEM.

The figure above shows the velocity streamlines through the orifice of the CA triple-dome and into the ear canal. Snapshots of the streamlines are taken at times 0.02, 0.08, 0.24, and 0.96 ms simulation time. As the flow develops, a swirling effect manifests in the ear canal, especially near the bottom of the canal near the TM. Although the current HEM does not include the HPC of the CA EP, it is possible that such information regarding the flow pattern throughout the EP and ear canal may be utilized to design orifice geometries capable of efficiently dissipating impulse energy, saving the ear from overpressure magnitudes that are currently deemed dangerous.

Chapter 5: Conclusion
5.1 Research Summary

There is a clear need for an advance analysis method capable of giving detailed information pertaining to the response of the human ear to blast impulse exposure. Additionally, hearing protection mechanisms must be explored and innovated such that soldiers may utilize military standard issue protection without hampering their effectiveness in combat. To provide a new means of evaluating human ear response to blast exposure and earplug function, the first human ear Finite Element model for high-intensity blast impulse analysis was created in Fluent/ANSYS Mechanical. Waveforms measured outside of the ear during human cadaver temporal bone experiments were applied to the Human Ear Model as input to the FE analyses. The model has shown the capability of accurately predicting pressure waveforms at key locations within the ear. The results from such analyses provide great detail of middle ear structural response to blast impulse exposures. Validated against experiments, the model was then shown to have applications in explaining observations made during experimentation. A conceptual model was constructed to conduct a preliminary parametric study of nonlinear earplug orifice geometry, and it was found that an ideal orifice construct may consist of multiple chambers separated by small-diameter contractions. The Human Ear Model for blast impulse analysis was then modified to include ear canal skin and linear and nonlinear earplugs. Analyses show that the model is capable of accurately predicting earplug function, although the material model for the foam earplug must be improved upon in order to simulate high-intensity impulse pressures. The Human Ear Model has proven effective in providing comprehensive computational analyses of high-intensity blast transduction through the ear while providing an unmatched level of detail of the response

of middle ear structures and of pressure and velocity volumetric data. This model and computational method shows great promise in providing enhanced means of evaluating Damage Risk Criteria of military weapons and weapon platforms and of designing and optimizing advanced Hearing Protection Devices.

5.2 Further Studies

In order to directly compare the Human Ear Model's effectiveness at predicting hearing loss to the Army's current prediction method (the AHAAH model), the cochlea with basilar membrane must be added to the model and the HEM must be shown capable of predicting hearing loss based on impulse waveforms and basilar membrane motion. A new mesh of the tympanic membrane to include the three composite layers that comprise the structure will provide a more detailed level of information regarding mode of tympanic membrane rupture.

A parametric study of orifice geometry effect must be conducted in the full HEM with a full representation of the nonlinear EP; EP function under blast impulse and hearing-level harmonic excitation must be well understood before the model may be applied to improve nonlinear EP design.

References

[1] "Benefits Report, Fiscal Year 2012," VA, 2012.

[2] G. Saunders and S. Griest, "Hearing loss in veterans and the need for hearing loss prevention programs," *Noise & Health,* vol. 11, no. 42, pp. 14-21, 2009.

[3] B. Amrein and T. Letowski, "High Level Impulse Sounds and Human Hearing: Standards, Physiology, Quantification," Report prepared for Human Research and Engineering Directorate , U.S. Army Research Laboratory, Aberdeen Proving Ground, MD, 2012.

[4] K. Yankaskas, "Prelude: Noise-induced tinnitus and hearing loss in the military," *Hearing Research,* vol. 395, pp. 3-8, 2013.

[5] G. Price, "Executive Summary of the Development and Validation of AHAAH," Report prepared for Human Research and Engineering Directorate, U.S. Army Research Laboratory, Aberdeen Proving Ground, MD, 2010.

[6] T. G. HFM-147, "Hearing Protection - Needs, Technologies and Performance," North Atlantic Treaty Organization, Research and Technology Organization, NATO, 2010.

[7] G. Price, "Critical Analysis and Comment on Patterson and Ahroon (2004) 'Evaluation of an auditory model using data from human volunteer studies' USAARL Report No. 2005-01," Technical Report 190805, Auditory Hazard Analysis, Charlestown, MD, 2005.

[8] K. Buck, "Performance of Different Types of Hearing Protectors Undergoing High-Level Impulse Noise," *JOSE,* vol. 15, no. 2, pp. 227-240, 2009.

[9] P. Fedele and J. Kalb, "Level-Dependent Nonlinear Hearing Protector Model in the Auditory Hazard Assessment Algorithm for Humans," Human Research and Engineering Directorate, U.S. Army Research Laboratory, Aberdeen Proving Grounds, MD, 2015.

[10] M. Grujicic, W. Bell, B. Pandurangan and e. al., "Fluid/Structure Interaction Computational Investigation of Blast-Wave Mitigation Efficacy of the Advance Combat Helmet," *J. of Materi Eng and Perform,* vol. 20, no. doi:10.1007/s11665-010-9724-z, p. 887, 2011.

[11] M. Grujicic, S. Ramaswami, J. Snipes and P. Dudt, "Potential improvement in helmet blast-protection via the use of a polyurea external coating: Combined experimental/computational analyses," *J. of Materials: Design and Applications,* no. doi: 10.1177/1464420716644472, pp. 1-31, 2016.

[12] S. Bailoor, R. Bjardwaj and T. Nguyen, "Effectiveness of eye armor during blast loading," *Biomech Model Mechanobiol,* vol. 14, no. doi: 10.1007/s10237-015-0667-z, pp. 1127-1237, 2015.

[13] G. Viallet, F. Sgard, F. Laville and H. Nelisse, "Investigation of the variability in earplugs sound attenuation measurements using a finte element method," *Applied Acoustics,* vol. 89, pp. 333-344, 2015.

[14] F. Sgard, M. Brummund, G. Viallet and e. al., "Prediction of airborne and structure borne sound transmission through hearing protectors using FEM," in *Inter-noise 2014*, Melbourne, Australia, 2014.

[15] G. Viallet, F. Sgard, F. Laville and J. Boutin, "A finite element model to predict the sound attenuation of earplugs in an acoustical test fixture," *J. Acoust. Soc. Am.,* vol. 136, pp. 1269-1280, 2014.

[16] G. Viallet, F. Sgard and F. Laville, "Development of a simplified axi-symmetric finite element model of the auditory canal occluded by an earplug: Variability of the attenuation as a function of the input parameters," *Canadian Acoustics,* vol. 39, no. 3, pp. 100-101, 2011.

[17] M. Brummund, F. Sgard, Y. Petit and e. al., "hree-dimensional finite element modeling of the human external ear: Simulation study of the bone conduction occlusion effect," *J. Acoust. Soc. Am. ,* vol. 135, no. 3, pp. 1433-1444, 2014.

[18] G. Viallet, G. Sgard, F. Laville and J. Boutin, "Axisymmetic versus three-dimensional finite element models for predicting the attenuation of earplugs in rigid walled ear canals," *J. Acoust. Soc. Am.,* vol. 134, no. 6, pp. 4470-4480, 2013.

[19] R. Gan, B. Feng and Q. Sun, "3-Dimensional finite element modeling of human ear for sound transmission," *Ann. Biomed. Eng.,* vol. 32, no. 6, pp. 847-856, 2004.

[20] X. Wang, T. Cheng and R. Gan, "Finite-element analysis of middle-ear pressure effects on static and dynamic behavior of the human ear," *J. Acoust. Soc. Am.,* vol. 122, no. 2, pp. 906-917, 2007.

[21] R. Gan, B. Reeves and X. Wang, "Modeling of sound transmission from ear canal to cochlea," *Ann. Biomed. Eng.,* vol. 35, no. 12, pp. 2180-2194, 2007.

[22] R. Gan, T. Cheng, C. Dai and F. Yang, "Finite element modeling of sound transmission with perforations of tympanic membrane," *J. Acoust. Soc. Am.,* vol. 126, no. 1, pp. 243-253, 2009.

[23] X. Zhang and R. Gan, "Finite element modeling of energy absorbance in normal and disordered human ears," *Hearing Research,* vol. 301, pp. 146-155, 2013.

[24] R. Gan, M. Wood and e. al., "A totally implantable hearing system - Design and function characterization in a 3D computational model and temporal bones," *Hearing Research,* vol. 263, no. 1-2, pp. 138-144, 2010.

[25] ANSYS, *ANSYS Workbench,* ANSYS Academic Research, Release 16.1.

[26] ANSYS, *Help System, ANSYS Workbench Documentation, Process Synchronization and Analysis Evolution,* ANSYS Academic Research, Release 16.1.

[27] B. Xia and D. Sun, "Applications of computational fluid dynamics in the food industry: a review," *Computers and Electronics in Agriculture,* vol. 34, pp. 5-24, 2002.

[28] S. V. Patankar, Numerical Heat Transfer and Fluid FLow, Hemisphere Publishing. ISBN 0891165223, 1980.

[29] ANSYS, Help System, Fluent Theory Guide, Basic Fluid, ANSYS Academic Research, Release 16.1.

[30] ANSYS, *Help System, Fluent Theory Guide, Multiphase,* ANSYS Academic Research, Release 16.1.

[31] ANSYS, *Help System, CFX Theory Guide, Basic Solver,* ANSYS Academic Research, Release 16.1.

[32] T. Koike, H. Wada and T. Kobayashi, "Modeling of the human middle ear using the finite-element method," *J. Acoust. Soc. Am.,* vol. 111, pp. 1306-1317, 2002.

[33] R. Gan, D. Nakmali, J. Xiao, K. Leckness and Z. Yokell, "Mechanical damage of tympanic membrane in relation to impulse pressure waveform - a study in chinchillas," *Hearing Research,* pp. 1-10, 2016.

[34] J. Altmann, "Acoustic Weapons - A prospective Assessment," *Science & Global Security,* vol. 9, pp. 165-234, 2001.

[35] R. Price, "Weapon Noise Exposure of the Human Ear Analyzed with the AHAAH Model," Human Research and Engineering Directorate, U.S. Army Research Laboratory, Aberdeen Proving Ground, MD, 2010.

[36] C. James, Finite Element Modeling and Exploration of Double Hearing Procetion Systems, Masters thesis: Virginia Polytechnic Institute and State University, 2006.

[37] L. J. Sivian, "Acoustic Impedance of Small Orifices," *J. Acoust. Soc. Am.,* vol. 7, no. 2, pp. 94-101, 1935.

[38] J. Zwislocki, "Wave Motion in the Cochlea Caused by Bone Conduction," *J. Acoust. Soc. Am.,* vol. 25, p. 986, 1953.

Appendix A: List of Abbreviations

AHAAH	Auditory Hazard Assessment Algorithm for Humans
AHU	Auditory Hazard Units
BP	Battle Plugs
CA	Combat Arms
CFD	Computational Fluid Dynamics
DRC	Damage Risk Criteria
EP	Earplug
FE	Finite Element
FEA	Finite Element Analysis
FEM	Finite Element Method
FSI	Fluid-Structure Interaction
FVM	Finite Volume Method
HEM	Human Ear Model
HPC	Hard Plastic Core
HPD	Hearing Protection Device
IL	Insertion Loss
IMJ	Incudo-Malleolar Joint
ISJ	Incudostapedial Joint
ME	Middle Ear
PDE	Partial Differential Equation
SAL	Stapedial Annular Ligament
SPL	Sound Pressure Level

TB	Temporal Bone
TM	Tympanic Membrane
TMA	Tympanic Membrane Annulus